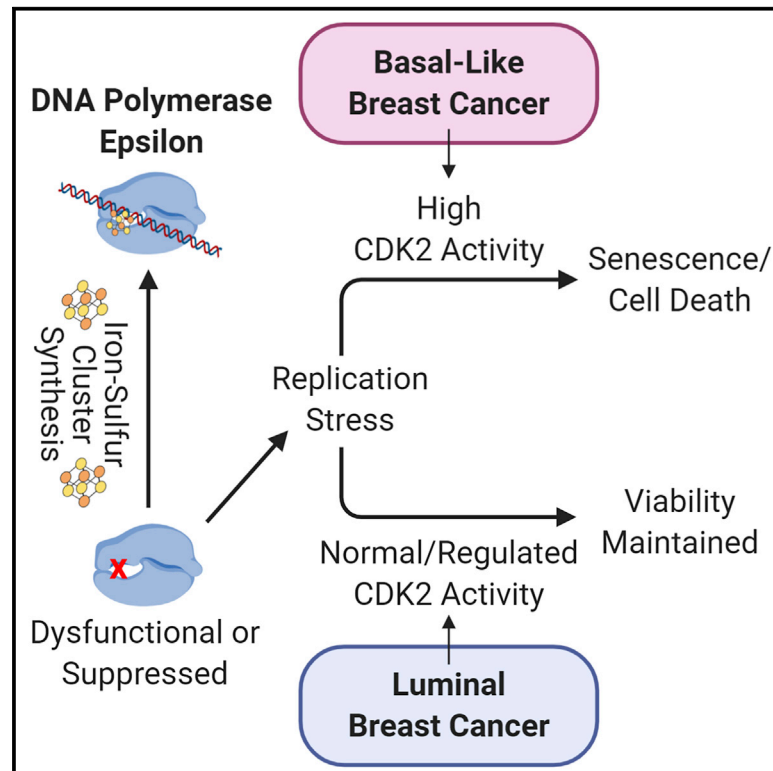


# Hyperactive CDK2 Activity in Basal-like Breast Cancer Imposes a Genome Integrity Liability that Can Be Exploited by Targeting DNA Polymerase $\epsilon$

## Graphical Abstract



## Authors

Vladislav O. Sviderskiy,  
Lili Blumenberg,  
Elizabeth Gorodetsky, ...,  
Sylvia Adams, Kelly V. Ruggles,  
Richard Possemato

## Correspondence

richard.possemato@nyulangone.org

## In Brief

Among breast cancer subtypes, basal-like breast cancer is particularly clinically intractable. Sviderskiy et al. identify DNA polymerase epsilon as the replicative polymerase upon which basal-like breast cancer particularly relies. Dependence on DNA polymerase epsilon is induced by CDK2 activation, and basal-like breast cancer tumors exhibit elevated phosphorylation of CDK2 targets.

## Highlights

- Iron-sulfur cluster synthesis is required for DNA replication
- Basal-like breast cancer is especially sensitive to DNA polymerase epsilon inhibition
- Patient basal-like breast cancer tumors have increased CDK2 target phosphorylation
- Activation of CDK2 enhances DNA polymerase epsilon dependence

Article

# Hyperactive CDK2 Activity in Basal-like Breast Cancer Imposes a Genome Integrity Liability that Can Be Exploited by Targeting DNA Polymerase $\epsilon$

Vladislav O. Sviderskiy,<sup>1,4</sup> Lili Blumenberg,<sup>2,4</sup> Elizabeth Gorodetsky,<sup>1,4</sup> Triantafyllia R. Karakousi,<sup>1,4</sup> Nicole Hirsh,<sup>1,4</sup> Samantha W. Alvarez,<sup>1,4</sup> Erdem M. Terzi,<sup>1,4</sup> Efiyenia Kaparos,<sup>1,4</sup> Gabrielle C. Whiten,<sup>1,4</sup> Shakirah Ssebyala,<sup>1,4</sup> Peter Tonzi,<sup>3,4</sup> Hannan Mir,<sup>1,4</sup> Benjamin G. Neel,<sup>2,4</sup> Tony T. Huang,<sup>3,4</sup> Sylvia Adams,<sup>4</sup> Kelly V. Ruggles,<sup>2,4</sup> and Richard Possemato<sup>1,4,5,\*</sup>

<sup>1</sup>Department of Pathology, New York University School of Medicine, New York, NY 10016, USA

<sup>2</sup>Department of Medicine, New York University School of Medicine, New York, NY 10016, USA

<sup>3</sup>Department of Biochemistry and Molecular Pharmacology, New York University School of Medicine, New York, NY 10016, USA

<sup>4</sup>Laura & Isaac Perlmutter Cancer Center, New York University School of Medicine, New York, NY 10016, USA

<sup>5</sup>Lead Contact

\*Correspondence: [richard.possemato@nyulangone.org](mailto:richard.possemato@nyulangone.org)

<https://doi.org/10.1016/j.molcel.2020.10.016>

## SUMMARY

Knowledge of fundamental differences between breast cancer subtypes has driven therapeutic advances; however, basal-like breast cancer (BLBC) remains clinically intractable. Because BLBC exhibits alterations in DNA repair enzymes and cell-cycle checkpoints, elucidation of factors enabling the genomic instability present in this subtype has the potential to reveal novel anti-cancer strategies. Here, we demonstrate that BLBC is especially sensitive to suppression of iron-sulfur cluster (ISC) biosynthesis and identify DNA polymerase epsilon (POLE) as an ISC-containing protein that underlies this phenotype. In BLBC cells, POLE suppression leads to replication fork stalling, DNA damage, and a senescence-like state or cell death. In contrast, luminal breast cancer and non-transformed mammary cells maintain viability upon POLE suppression but become dependent upon an ATR/CHK1/CDC25A/CDK2 DNA damage response axis. We find that CDK1/2 targets exhibit hyperphosphorylation selectively in BLBC tumors, indicating that CDK2 hyperactivity is a genome integrity vulnerability exploitable by targeting POLE.

## INTRODUCTION

Despite increased screening and improved treatments, breast cancer remains the second-leading cancer-related cause of mortality in women (Siegel et al., 2016). Once considered a single disease, breast cancer is now appreciated to consist of four common molecular subtypes: luminal A, luminal B, HER2E, and basal-like (Koboldt et al., 2012). Of these, basal-like tumors display frequent and early relapse and have a relatively poor five-year prognosis, partly because no targeted therapies exist for this subtype, which accounts for 15%–25% of all cases (Bertucci et al., 2012). As such, identification of novel targetable liabilities and treatments is necessary to improve outcomes for these patients.

The study of altered tumor metabolism and genomic instability, two cancer hallmarks, has driven our knowledge about the transformed state and led to the discovery of anti-cancer therapies (Hanahan and Weinberg, 2011). By hampering genomic stability and altering metabolism, cancer cells develop the capacity to evolve and survive in the tumor microenvironment (Lord and Ashworth, 2012; Vander Heiden and DeBerardi-

nis, 2017). However, these adaptations also produce targetable vulnerabilities such as the sensitivity of *BRCA1* and *BRCA2* mutated tumors to PARP inhibitors (Lord and Ashworth, 2017). Several studies have also demonstrated that inhibition of reprogrammed pathways or deprivation of tumor-essential nutrients can suppress tumor growth (Birsoy et al., 2014; DeBerardinis and Chandel, 2016; Rimawi et al., 2015). To uncover novel tumor liabilities, we identified molecular oxygen ( $O_2$ ) levels as a major driver of cancer metabolic dependency and found that elevated  $O_2$  environments create a reliance on iron-sulfur cluster (ISC) biosynthesis, a promising, understudied target that we find to be at the intersection of metabolism and genomic stability (Alvarez et al., 2017).

ISCs are cell-essential cofactors that support the function of at least 48 proteins involved in diverse cellular processes, such as energy metabolism, iron homeostasis, DNA replication, and DNA repair (Netz et al., 2014; Stehling et al., 2014). To support these functions, ISCs act as electron carriers, sulfur donors, catalysts in chemical reactions, regulatory sensors, and stabilizers of protein domains (Beinert et al., 1997; Maio and Rouault, 2015). Synthesis, maturation, and then insertion of

the cofactor into apoproteins comprises a coordinated process encompassing some 30 proteins (Netz et al., 2014). Canonically, this process begins in the mitochondrial matrix and involves the key enzyme NFS1, a cysteine desulfurase that removes sulfur from the amino acid cysteine and donates it to ISC cofactor formation.

The NFS1 locus undergoes positive selection in lung adenocarcinomas, and incipient lung tumors and metastases require robust ISC biosynthesis (Alvarez et al., 2017). Molecular oxygen can damage ISCs, and as a result, cancer cells depend more acutely on ISC biosynthesis to replenish cofactor pools at elevated  $O_2$  concentrations (e.g., those found in lung airways or standard cell culture) compared with tissue  $O_2$  levels. Suppression of NFS1 at atmospheric  $O_2$  levels leads to dysfunction of pathways dependent on ISC holoenzymes such as the electron transport chain (ETC) and iron homeostasis (Alvarez et al., 2017). However, the pathway or proteins most responsible for proliferation defects upon ISC synthesis inhibition in cancer remain unknown.

In yeast, mitochondrial ISC biosynthesis is required for maintenance of nuclear genome integrity (Veatch et al., 2009). Accordingly, several DNA replication and DNA repair proteins harbor an ISC, although the molecular role of these cofactors mostly remains unknown (Gari et al., 2012; Paul and Lill, 2015; Stehling et al., 2012). Included in these ISC-dependent DNA metabolism proteins are the three main polymerases of nuclear DNA replication, polymerase alpha (Pol  $\alpha$ ), polymerase delta (Pol  $\delta$ ), and polymerase epsilon (Pol  $\epsilon$ ) (Netz et al., 2011). Pol  $\alpha$ , along with the primase complex, initiates replication on both strands by adding RNA primers, allowing Pol  $\epsilon$  and Pol  $\delta$  to catalyze leading- and lagging-strand replication, respectively (Burgers and Kunkel, 2017). These polymerases contain a putative ISC binding site at their C terminus (Netz et al., 2011). ISC binding in Pol  $\delta$  stabilizes the protein and allows for interaction with other Pol  $\delta$  subunits, but for Pol  $\alpha$  and Pol  $\epsilon$ , the role of cofactor binding at the C terminus is not thoroughly established or characterized (Baranovskiy et al., 2012; Netz et al., 2011). Unlike the other polymerases, Pol  $\epsilon$  has a second ISC binding site within its polymerase domain that is important for polymerase activity (Jain et al., 2014; Ter Beek et al., 2019). These findings suggest that inhibition of ISC biosynthesis could affect DNA replication and genomic stability.

Before executing the genomically high-risk events of DNA replication and mitosis, cells employ cell-cycle checkpoints controlled by the activity of cyclin-dependent kinases (CDKs) (Morgan, 1997). CDK1 and CDK2 (CDK1/2) regulate the G1/S and G2/M transitions, respectively, and their activity is inhibited upon activation of DNA damage response pathways to block cell-cycle progression (Otto and Sicinski, 2017). Genomic profiling of human tumors has demonstrated frequent dysregulation of CDK-dependent cell-cycle control mechanisms in human cancers (Deshpande et al., 2005). Oncogenic activation of CDK4 and CDK6 (CDK4/6) occurs in luminal breast cancer (LUBC), and CDK4/6 inhibitors (CDK4/6i) have clinical utility in this tumor type (Turner et al., 2018). In contrast, basal-like breast cancer (BLBC) tumors have multiple genomic alterations that could promote CDK2 activity, including p53 mutations, cyclin E overexpression, and c-Myc activation (Koboldt et al., 2012).

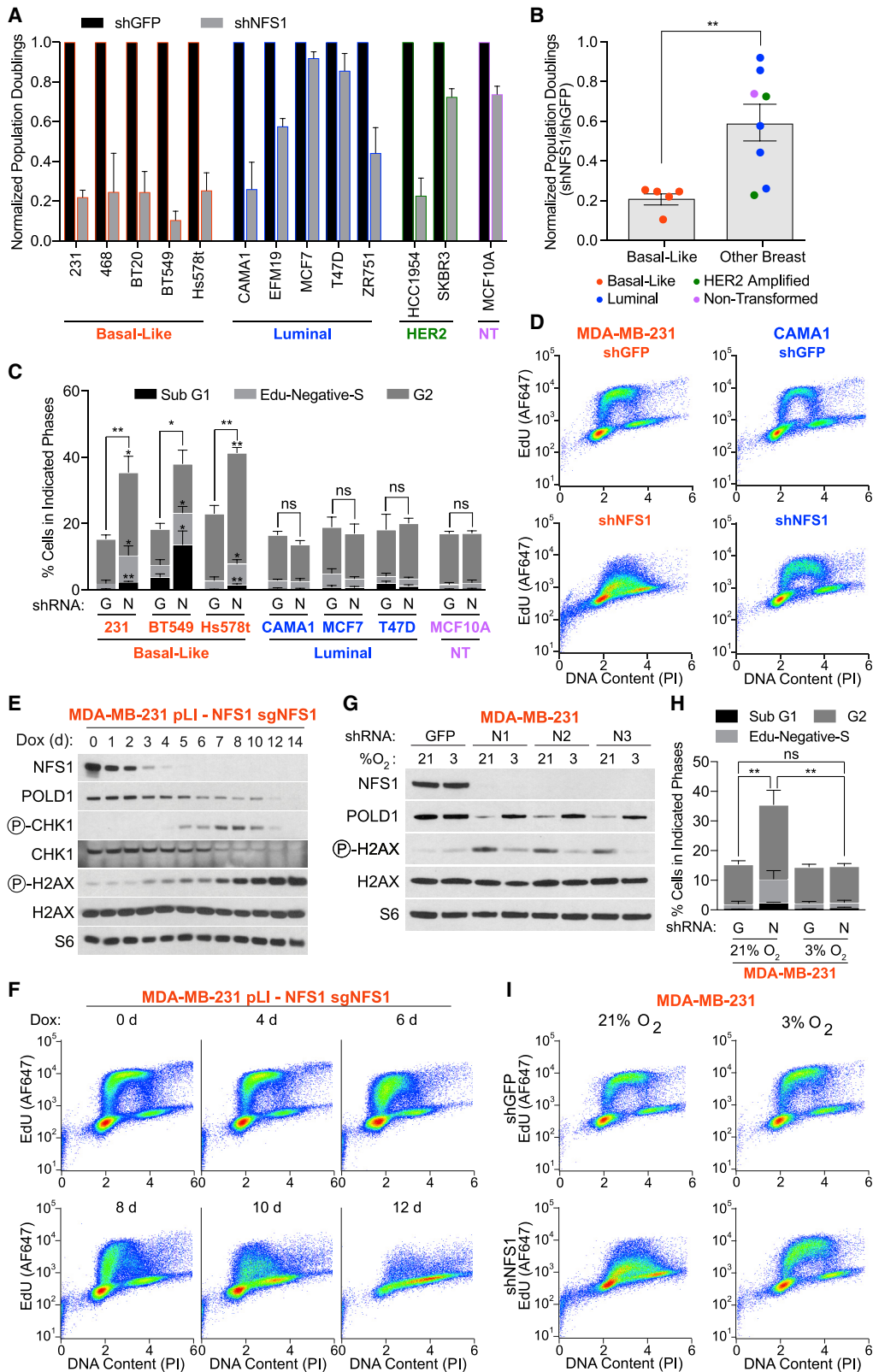
Here, we discover that BLBC cell lines are particularly sensitive to suppression of ISC biosynthesis compared with cell lines derived from other breast cancer subtypes and non-transformed mammary epithelial cells. We demonstrate that a major role of ISC biosynthesis in BLBC cells is to support DNA replication and Pol  $\epsilon$  function and that suppression of either ISC biosynthesis or Pol  $\epsilon$  in BLBC leads to DNA damage caused by replication stress, defined as the slowing or stalling of replication fork progression (Zeman and Cimprich, 2014). Inhibitors that affect CDK2 activity can modulate sensitivity to Pol  $\epsilon$  suppression, and we provide evidence of intrinsic CDK2 hyperactivation in BLBC that may contribute to its enhanced sensitivity to inhibition of ISC biosynthesis or Pol  $\epsilon$  function.

## RESULTS

### Partial Suppression of ISC Biosynthesis Leads to Severe Proliferation Defects, Cell-Cycle Arrest, and DNA Damage in BLBC Cells

Breast cancer cells require the key ISC biosynthetic enzyme NFS1 to form metastatic lung tumors (Alvarez et al., 2017). These findings prompted us to evaluate the sensitivity of human breast cancer cell lines to ISC biosynthesis suppression. We expressed a short hairpin RNA (shRNA) targeting NFS1 (shNFS1) or a non-targeting shRNA (shGFP) in BLBC cell lines (MDA-MB-231, MDA-MB-468, BT-20, BT-549, and Hs578t), LUBC cell lines (MCF7, T47D, EFM-19, CAMA-1, and ZR-75-1), Her2-amplified breast cancer cell lines (SK-BR-3 and HCC1954), and a non-transformed cell line derived from human mammary epithelium (MCF10A). BLBC cell lines demonstrated significantly stronger growth inhibition upon NFS1 suppression compared with other subtypes (Figures 1A and 1B). We also profiled cell-cycle state by monitoring DNA content and incorporation of a thymidine analog (5-Ethynyl-2-deoxyuridine, EdU). Upon NFS1 suppression, BLBC cell lines, but not LUBC or non-transformed cell lines, exhibited an accumulation of cells in three populations: (1) EdU-negative cells with S-phase DNA content (EdU-negative-S), (2) cells in G2 phase, and (3) cells with sub-G1 DNA content, consistent with apoptotic cells (Figures 1C, 1D, S1A, and S1B). These data indicate that the loss of proliferative capacity observed upon NFS1 suppression in BLBC cells is caused by BLBC-specific defects in progression past the G1/S transition. Indeed, despite a substantial reduction in proliferation of LUBC cell line CAMA-1 upon NFS1 suppression, we observed minimal changes to its cell-cycle profile (Figures 1C and 1D).

We considered the possibility that BLBC cells are differentially affected by ISC synthesis suppression as a result of differences in residual ISC biosynthetic activity despite expression of shNFS1. Suppression of NFS1 in all subtypes led to depletion of ISC proteins whose stability depends on ISC binding (POLD1, a nuclear protein, and ferrochelatase [FECH], a mitochondrial protein), consistent with reduction of ISC pools across subcellular compartments independent of breast cancer subtype (Figure S1C). In all subtypes, suppression of NFS1 also led to phenotypes consistent with loss of an ISC from the iron-response protein IRP1: an increase in transferrin receptor (TFRC) protein levels, a decrease in ferritin heavy-chain protein levels, and a loss of aconitase activity (Figures S1C and S1D).



(legend on next page)

We conclude that breast cancer subtypes exhibit loss of ISC biosynthesis to a similar degree upon shNFS1 expression, which does not correlate with subtype-specific changes in proliferative capacity.

To temporally study effects of acute ISC synthesis loss independent of RNAi, we engineered BLBC MDA-MB-231 cells that express a small guide RNA (sgRNA)-resistant, doxycycline (DOX)-repressible NFS1 cDNA and then disrupted the endogenous NFS1 locus by CRISPR-Cas9. Addition of DOX reduced NFS1 protein to undetectable levels within 5 days and results in a decrease in levels of POLD1 (Figures 1E and S1E). Concurrently, we observed a gradual reduction in EdU incorporation and accumulation of cells in the EdU-negative-S and G2 populations, similar to shNFS1 expression. By day 12, EdU incorporation was undetectable in nearly all cells (Figures 1F and S1F). These defects indicate that DNA replication is affected by ISC synthesis inhibition. As a result, we assayed markers of replication fork stalling (phosphorylation of Chk1 at S345 [pCHK1]) and DNA damage (H2AX phosphorylation at S139, or  $\gamma$ -H2AX) and observed that their levels are increased concomitant with induction of cell-cycle defects (Figures 1E, 1F, S1E, and S1F). Suppression of NFS1 in the panel of breast cell lines revealed substantial increases in  $\gamma$ -H2AX in all five BLBC lines tested but only one non-BLBC line (Figure S1C). These data indicate that ISC biosynthesis supports DNA replication and that ISC synthesis suppression results in persistent DNA damage selectively in BLBC.

Because O<sub>2</sub> degrades ISCs, culturing cells at tissue-level O<sub>2</sub> concentrations (3%) rather than atmospheric O<sub>2</sub> levels (21%) rescues proliferation defects induced by ISC biosynthesis inhibition (Alvarez et al., 2017). As such, if ISC inhibition limits cell proliferation because of suppressing replication, we would expect phenotypes of replication inhibition to also be suppressed at tissue oxygen levels. Indeed, culturing cells expressing NFS1 shRNAs at 3% O<sub>2</sub> prevented loss of POLD1 protein, restored cell-cycle profiles, and rescued  $\gamma$ -H2AX levels (Figures 1G–1I).

### ISC Binding Sites in the Replicative DNA Polymerases Are Required for Proliferation and Prevention of DNA Damage in BLBC

We hypothesized that the selective proliferation defect in BLBC upon NFS1 inhibition stems from dysfunction of ISC-dependent

DNA metabolism processes or proteins. Purine and pyrimidine biosynthesis has ISC-dependent biosynthetic steps (catalyzed by PPAT and DHODH), which can be rescued by hypoxanthine and uridine supplementation. However, adding these downstream metabolites did not rescue proliferation or cell-cycle defects caused by NFS1 suppression (Figures S2A and S2B). The ETC also depends upon ISC proteins for electron transfer reactions, and treatment with pyruvate and uridine can rescue loss of cell viability caused by ETC defects. Although these additives restored cell viability upon treatment with complex III inhibitor antimycin A, they did not restore proliferation of NFS1-suppressed BLBC cell lines (Figures S2A and S2C). Furthermore, ETC-defective cells retain sensitivity to NFS1 suppression (Alvarez et al., 2017). Therefore, inhibition of nucleotide metabolism or ETC alone is not sufficient to explain the loss of cell viability or cell-cycle defects observed upon ISC biosynthesis inhibition.

We next considered whether abrogation of one of the 14 ISC-containing DNA metabolism proteins drives the differential requirement for ISC biosynthesis in BLBC. We suppressed these 14 targets using two independent shRNAs in two LUBC and two BLBC cell lines. Of these genes, *POLE1*, which encodes POLE, the catalytic subunit of the leading-strand DNA polymerase holoenzyme Pol  $\epsilon$ , emerged as the most differentially required in BLBC lines (Figure S2D; Table S1). We then consulted publicly available gene essentiality data based on pooled RNAi loss-of-function genetic screens (Tsherniak et al., 2017). Genes whose pattern of essentiality correlates across this dataset typically target important related biological processes or multi-protein complexes. For example, the patterns of sensitivity to suppression of the core ISC biosynthesis machinery (e.g., *NFS1*, *ISCU*, *ABCB7*, and *FXN*) are highly correlated. We found that of proteins that use ISCs as a cofactor, the phenotype of *POLE1* suppression best correlates to suppression of these ISC biosynthetic proteins ( $r = 0.404$  and  $p = 4e-21$  for *POLE1* and *ISCU*); *POLA1* and *POLD1* also exhibited a significant correlation ( $r = 0.327$  and  $p = 6e-14$  for *POLA1* and *ISCU* and  $r = 0.248$  and  $p = 2e-8$  for *POLD1* and *ISCU*) (Figure 2A; Table S2). Moreover, two independent loss-of-function genetic screens performed in breast cancer cell lines identify POLE as the ISC-containing protein most differentially required in BLBC (Marcotte et al., 2016; Tsherniak et al., 2017) (Figure S2E).

### Figure 1. Partial Suppression of Iron-Sulfur Cluster Biosynthesis Leads to Severe Proliferation Defects, Cell-Cycle Arrest, and DNA Damage in BLBC Cells

(A) Population doublings (5–9 days) of cell lines infected with non-targeting shRNA (shGFP, black bars) or shRNA targeting NFS1 (shNFS1, gray bars), relative to shGFP. Cell lines are grouped based on classification: basal-like (orange), luminal (blue), Her2 amplified (HER2, green), or non-transformed (NT, purple).

(B) Data from (A) grouped by basal-like or not basal-like.

(C) Quantification of cell-cycle analysis for cell lines expressing shGFP (G) or shNFS1 (N). Classification based on EdU incorporation and propidium iodide (PI) staining intensities as in Figure S1A. EdU-Negative-S, EdU-negative cells with S-phase DNA content. Asterisks indicate significance comparing subcategories individually (above error bars) and sum of proportions (above stacked bars).

(D) Representative cell-cycle profiles 7 days after shRNA infection. EdU incorporation and DNA content (PI) by flow cytometry.

(E) Immunoblots for the indicated proteins or modifications. Lysates from MDA-MB-231 clone with endogenous NFS1 deletion expressing DOX-repressible NFS1 cDNA. Days of DOX (0.5  $\mu$ g/mL) treatment are indicated. CHK1 phosphorylation occurs at S345, and H2AX phosphorylation occurs at S139.

(F) Representative cell-cycle profiles of cells from (E) upon DOX addition for the indicated days, as in (D).

(G) Immunoblots for the indicated proteins or modifications. Lysates isolated from MDA-MB-231 cells infected with shGFP (GFP) or shNFS1 (N1, shNFS1\_1; N2, shNFS1\_2; N3, shNFS1\_3) and cultured at the indicated O<sub>2</sub> concentration (% O<sub>2</sub>) 7 days after infection.

(H) Quantification of cell-cycle profiles in (I).

(I) Representative cell-cycle profiles as in (D) 7 days after shRNA infection of MDA-MB-231 cells cultured at the indicated O<sub>2</sub> concentration.

\* $p < 0.05$ , \*\* $p < 0.01$ ; ns, not significant. Error bars are SEM.  $n = 3$  independent experiments. See also Figure S1.

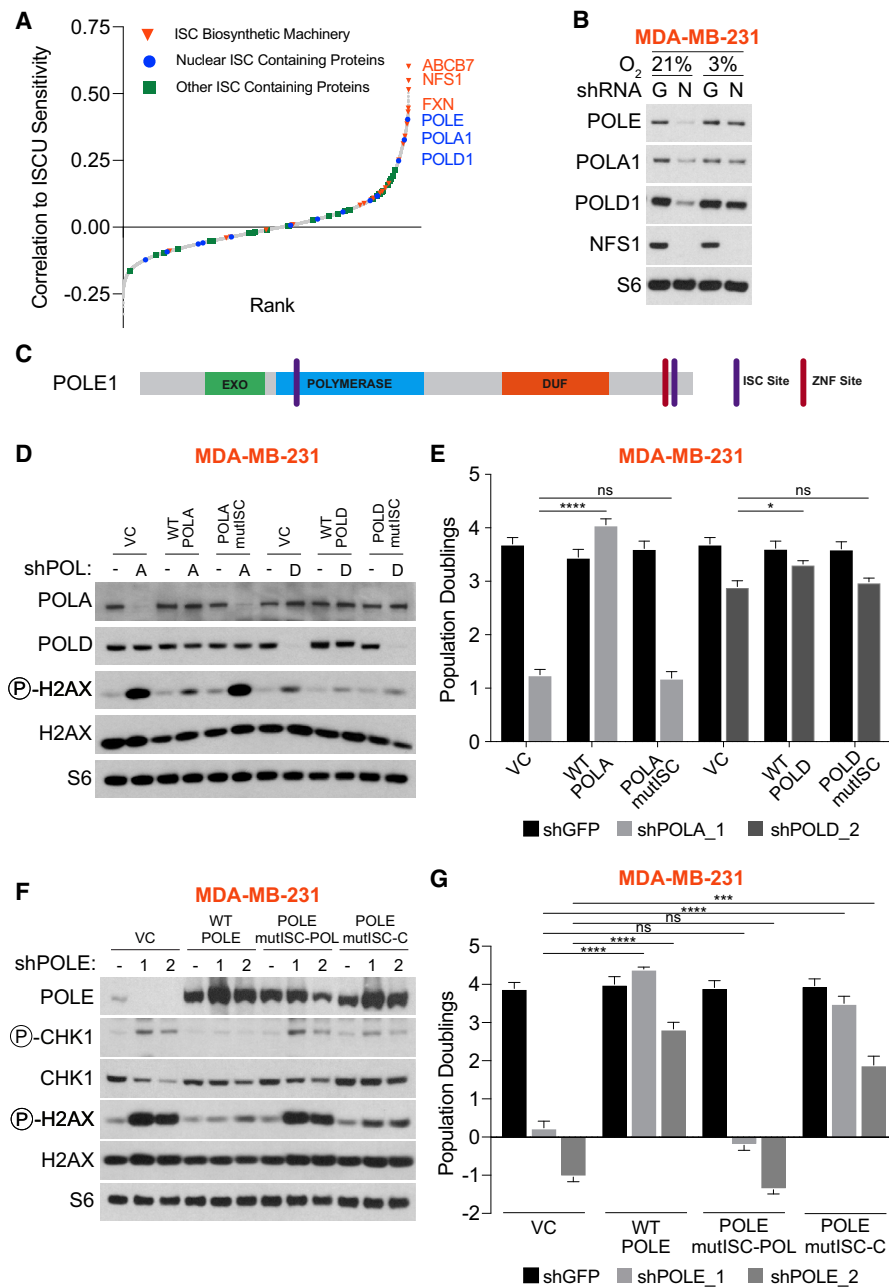


**Figure 2. ISC Binding Sites in the Replicative DNA Polymerases Are Required for Proliferation and Prevention of DNA Damage in BLBC**

(A) Rank-ordered Pearson correlation coefficients for sensitivity to ISCU inhibition versus inhibition of a given gene in cell lines from the Cancer Cell Line Encyclopedia. ISC biosynthetic machinery (orange triangles), nuclear ISC-containing proteins (blue circles), and other ISC-containing proteins (green squares) are indicated. The most significant genes are annotated.

(B) Immunoblots for the indicated proteins or modifications. Lysates isolated from MDA-MB-231 cells 7 days after infection with shGFP (G) or shNFS1\_1 (N) and cultured at the indicated O<sub>2</sub> concentration (% O<sub>2</sub>).

(C) POLE1 protein diagram indicating major domains (EXO, exonuclease; polymerase; DUF, domain of unknown function) and location of ISC (ISC site) or zinc finger (ZNF site).

(D) Immunoblots for the indicated proteins or modifications. Lysates isolated from MDA-MB-231 cells infected with vector control (VC) or constructs encoding WT POLA1, WT POLD1, or ISC site mutants (POLA ISCmut or POLD ISCmut), followed by infection with shGFP (–) or shRNAs targeting POLA (shPOLA\_1, A) or POLD (shPOLD\_2, D), 6 days after shRNA infection.

(E) Population doublings (5 days) of cell lines in (D).

(legend continued on next page)

Based on these data, we explored the function of ISCs in POLA1, POLD1, and POLE. Upon NFS1 suppression, we observed a reduction in the levels of all three proteins, which was rescued by culturing cells at 3% O<sub>2</sub> (Figure 2B). These data indicate that ISC cluster binding of all three replicative polymerases is linked to protein stability.

If ISC synthesis maintains cell viability by supporting polymerase function, residues in POLA1, POLD1, and POLE that coordinate ISCs should be essential for cell viability (Figure 2C). We expressed shRNA-resistant cDNAs (wild-type [WT] POLA, WT POLD, or WT POLE) or mutants in which the cysteine residues that coordinate each ISC cofactor have been mutated to serine (POLA mutISC, POLD mutISC, POLE mutISC-POL, and POLE mutISC-C), followed by suppression of the endogenous polymerase. Expression of an shRNA targeting *POLA1* reduced *POLA1* protein levels, increased  $\gamma$ -H2AX levels, and reduced proliferative capacity, effects rescued by expression of WT POLA, but not POLA mutISC (Figures 2D, 2E, S2F, and S2G). Expression of an shRNA targeting *POLD1* (shPOLD\_2) substantially reduced *POLD1* protein levels but did not consistently increase  $\gamma$ -H2AX levels and led to modest reduction in proliferative capacity (Figures 2D, 2E). The effects of *POLD1* suppression on *POLD* protein levels and proliferative capacity were partially rescued by expression of WT POLD, but not POLD mutISC (Figures 2D, 2E). Expression of WT POLE rescued both proliferation defects and DNA damage induced by shPOLE expression (Figures 2F and 2G). POLE mutISC-C also rescued this proliferation defect and DNA damage almost completely, but POLE mutISC-POL was unable to rescue either phenotype, demonstrating that cysteine residues that coordinate the polymerase domain cofactor are required for POLE to maintain cell viability (Figures 2F and 2G). Consistent with ISC-dependent changes in protein stability, we did not observe an increase in *POLA1* or *POLD1* protein levels upon expressing POLA mutISC and POLD mutISC (Figure 2D). In contrast, mutation of a single POLE ISC site still resulted in stably expressed protein (Figure 2F). These data demonstrate that ISC binding sites are required for each of the three replicative polymerases to maintain cell viability and, in the cases of POLE and *POLA1*, to prevent DNA damage.

In *S. cerevisiae*, the polymerase domain POLE ISC supports polymerase function, but the role of the C-terminal ISC has not been fully characterized. Structural data suggest that the C-terminal ISC mediates the interaction with the POLE2 subunit (Baranovskiy et al., 2017), which integrates POLE into replisomes (Sengupta et al., 2013). To explore the requirement for this interaction, we immunoprecipitated FLAG-tagged POLE or its ISC mutants and immunoblotted hemagglutinin (HA)-tagged POLE2. Although WT POLE and POLE mutISC-POL interacted with POLE2, POLE mutISC-C and POLD did not, implicating the C-terminal ISC binding site in the POLE2 interaction (Figure S2H). Suppression of POLE2 in MDA-MB-231 cells caused an increase in DNA damage markers and partial blunting of pro-

liferation, phenotypes rescued by expressing HA-POLE2 (Figures S2I–S2K). Therefore, although POLE2 is cell essential, the POLE:POLE2 interaction mediated by the C-terminal ISC binding site is not strictly required for cell viability. Indeed, yeast harboring equivalent mutations in the POLE C-terminal ISC binding site display normal growth kinetics (Dua et al., 1999).

### Suppression of *POLE1* Limits Growth and Induces Cell-Cycle Defects in BLBC Cells but Not LUBC Cells

We next considered whether BLBC cell lines exhibit a selective requirement for these replicative polymerases. We expressed either a control shRNA (shGFP) or shRNAs targeting *POLE1*, *POLA1*, or *POLD1* in an expanded panel of breast cancer cell lines and assayed proliferation. In all cell lines tested, suppression of *POLA* caused loss of cell viability and an increase in  $\gamma$ -H2AX, whereas suppression of *POLD* resulted in minimal effects (Figure S3A).

In contrast, *POLE* suppression led to severe growth defects in BLBC cell lines, but not in LUBC cell lines or the non-transformed MCF10A cell line (Figures 3A and 3B). Moreover, *POLE* suppression in BLBC, but not in LUBC, cell lines led to accumulation of EdU-negative-S<sub>2</sub> cells in G<sub>2</sub>, and cells with sub-G<sub>1</sub> DNA content, similar to NFS1 suppression (Figures 3C, 3D, and S3B). We then assessed whether the requirement for *POLE* was associated with curated phenotypes using public data. Across breast cancer cell lines, we calculated the Pearson correlation coefficient (*r*) between a metric of *POLE1* essentiality and the expression of each gene, generating a ranked gene list that we examined by gene set enrichment analysis (GSEA). We observed that expression of basal markers highly correlates with sensitivity to *POLE* suppression and that expression of luminal markers highly correlates with resistance (Figure 3E; Table S3). These data demonstrate that BLBC cells are selectively unable to tolerate reduced levels of *POLE*, an observation that does not extend to the other replicative polymerase catalytic subunits, *POLA* and *POLD*.

A key therapeutic advantage of targeting an ISC protein like *POLE* compared with the ISC biosynthetic machinery is that inhibition of an ISC protein should affect protein function independent of environmental O<sub>2</sub> tension. Indeed, the effects of *POLE1* suppression are not restored by low O<sub>2</sub> culture (Figure S3C). Because of its O<sub>2</sub>-independent effect, we hypothesized that direct *POLE* suppression, unlike NFS1 suppression, should affect primary tumor growth. Consequently, we generated MDA-MB-231 cells containing a DOX-inducible shPOLE\_1 and expressing an shRNA-resistant WT-*POLE* cDNA (shPOLE Rescue) or vector control (shPOLE VC) and injected these cells into the 4<sup>th</sup> murine mammary fat pad. Upon formation of palpable tumors, mice were transitioned to DOX chow. shPOLE VC tumors exhibited diminished *POLE* protein levels after DOX addition, whereas shPOLE Rescue tumors maintained *POLE* levels (Figure S3D). Although shPOLE Rescue tumors maintained

(F) Immunoblots for the indicated proteins or modifications. Lysates isolated from MDA-MB-231 cells infected with VC or constructs encoding WT *POLE* or *POLE* with mutations in the ISC site located in the polymerase domain (*POLE* mutISC-POL) or near the C terminus (*POLE* mutISC-C), followed by infection with shGFP (–) or shRNAs targeting *POLE* (1 or 2), 6 days after shRNA infection.

(G) Population doublings (5 days) of cell lines in (E).

\**p* < 0.05, \*\*\**p* < 0.001, \*\*\*\**p* < 0.0001; ns, not significant. Error bars are SEM. *n* ≥ 3 independent experiments. See also Figure S2 and Table S2.

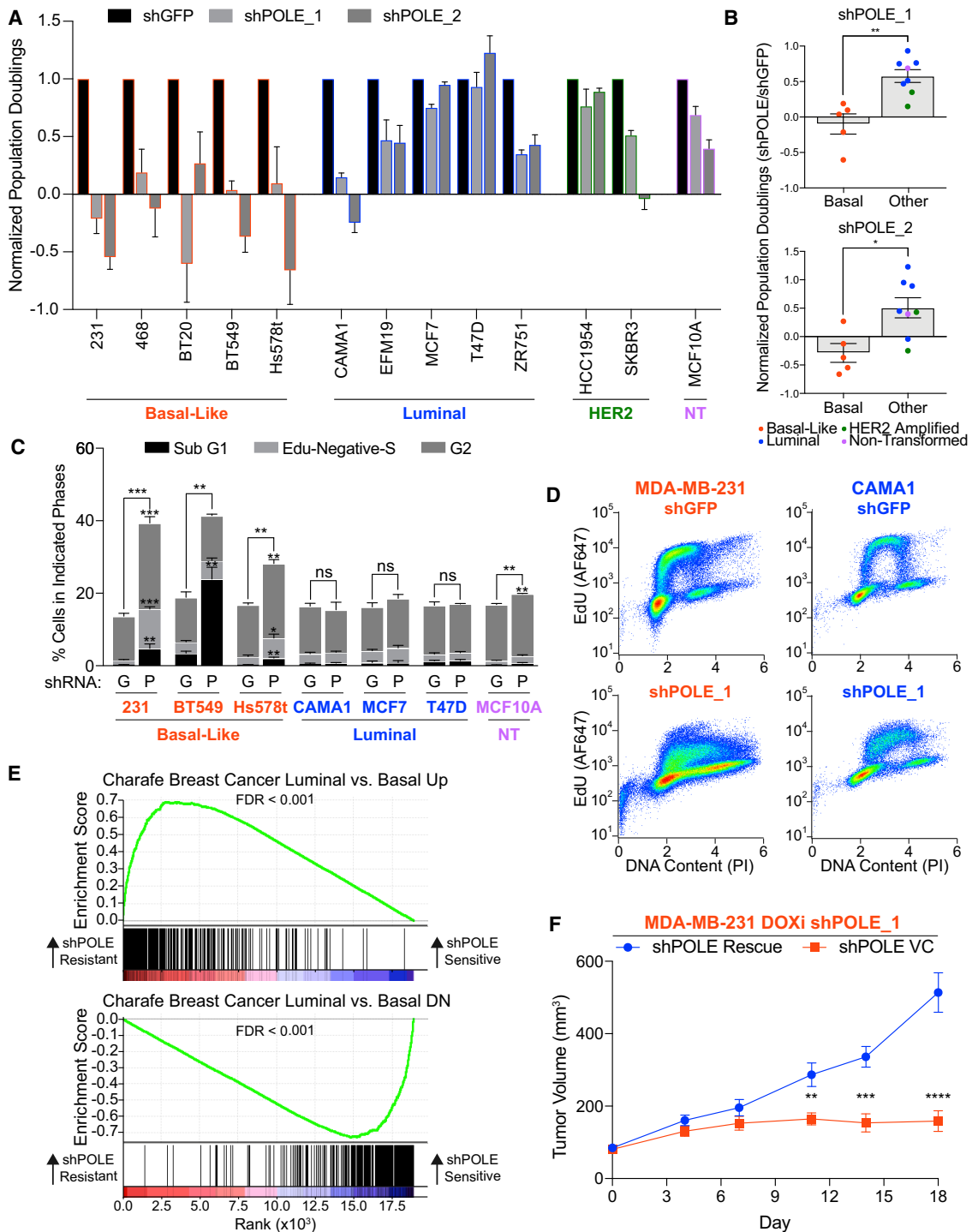


**Figure 3. Suppression of *POLE1* Limits Growth and Induces Cell-Cycle Defects in BLBC Cells but Not LUBC Cells**

(A) Population doublings (5–9 days) of the indicated cell line infected with shGFP (black bars) or shRNAs targeting POLE (shPOLE\_1 and shPOLE\_2, gray bars), relative to shGFP. Cell lines are grouped based on classification: basal-like (orange), luminal (blue), Her2 amplified (HER2, green), or non-transformed (NT, purple).

(B) Data from (A) grouped by basal-like or not basal-like.

(C) Quantification of cell-cycle analysis for the indicated cell lines expressing non-targeting shGFP (G) or shPOLE\_1 (P). Classification based on EdU incorporation and PI staining intensities (Figure S1A). Asterisks indicate significance comparing subcategories individually (above error bars) and the sum of proportions (above stacked bars).

(D) Representative cell-cycle profiles of cell lines 6 days after shRNA infection. EdU incorporation and DNA content (PI) by flow cytometry.

(legend continued on next page)

growth upon DOX addition, shPOLE VC tumors exhibited strong reduction in tumor growth, which ceased after seven days of treatment (Figure 3F). Therefore, unlike NFS1, POLE suppression can inhibit primary tumor growth at the  $O_2$  concentration found in mammary fat pad xenograft tumors.

### POLE Suppression Leads to DNA Damage, Replication Fork Stalling, and Induction of Replicative Senescence in BLBC Cells

Because we observe cell-cycle defects upon NFS1 or POLE suppression specifically in BLBC, we hypothesized that POLE suppression induces phenotypes associated with a loss of genomic integrity in BLBC. Upon POLE suppression, we observed significantly increased levels of pCHK1 and  $\gamma$ -H2AX in all five BLBC cell lines tested but only one of eight other lines (Figure 4A). Unlike POLE suppression, treatment with the alkylating agent methyl methanesulfonate (MMS) increased  $\gamma$ -H2AX and pCHK1 in both LUBC and BLBC cell lines, indicating that LUBC cells have the capacity to phosphorylate these targets but do not progress to  $\gamma$ -H2AX accumulation in response to POLE suppression (Figure S4A). To further test the response to replicative stress in these cell lines, we treated BLBC cell line MDA-MB-231 and LUBC cell line MCF7 with no, low-dose (0.2 mM) or high-dose (2 mM) hydroxyurea (HU) for 4, 24, or 48 h, followed by drug washout and assessment of recovery. HU inhibits ribonucleotide reductase, leading to depletion of deoxyribonucleotide triphosphate (dNTP) levels and replication stress. Indeed, we observe pCHK1 upon HU treatment within 4 h in both lines (Figure S4B). Low-dose HU treatment followed by withdrawal does not affect post-withdrawal proliferative capacity, whereas high-dose HU treatment inhibits proliferative capacity to a similar degree in both lines (Figure S4C). These data indicate that the LUBC and BLBC cell lines are competent to signal and recover from HU-induced replication stress despite differential sensitivity to POLE inhibition. This finding suggests a fundamental difference between the effect of general replication stress and that of low POLE levels.

We next assayed nuclear single-stranded DNA (ssDNA) levels in two BLBC and LUBC cell lines and the non-transformed cell line MCF10A. Cells were treated with the thymidine analog bromodeoxyuridine (BrdU), and incorporation was measured by immunofluorescence under non-denaturing conditions. Using this protocol, anti-BrdU antibody binding occurs only when exposed ssDNA exists, as commonly observed when replication forks stall. We observed significant anti-BrdU focus formation only in the BLBC cell lines upon POLE suppression (Figures 4B and 4C). In addition, transcriptomic analysis of POLE-suppressed BLBC cells supports stalling in S phase. MDA-MB-231 cells, but not MCF7 or CAMA1 cells, demonstrate a decrease in transcripts that are associated with G2/M phase of the cell cycle upon POLE suppression (Figures S4D and S4E; Table S4). These data demonstrate that POLE suppression induces replication fork stalling and cell-

cycle arrest in S phase, specifically in BLBC cells. To assess replication at individual replication forks upon POLE suppression, we performed DNA fiber analysis on the BLBC cell lines MDA-MB-231 and Hs578t and the luminal cell line MCF7. We observed that MCF7 cells increased replication speed upon POLE suppression, similar to effects previously seen in fibroblasts of patients with *POLE1* hypomorphic mutations (Figure S4F) (Bellelli et al., 2018). In contrast, BLBC cell lines demonstrated either similar or slower replication kinetics upon POLE suppression.

Transcriptomic analysis also revealed that suppression of POLE in MDA-MB-231, but not LUBC, cell lines leads to an increase in cytokine transcripts targeted by the nuclear factor  $\kappa$ B (NF- $\kappa$ B) transcription factor (Figures 4D and 4E; Table S4). A subset of these transcripts is induced during replicative senescence as part of the senescence-associated secretory phenotype (SASP). qPCR in an expanded panel of breast cancer cell lines confirmed robust increases in several SASP transcripts (CSF3, interleukin (IL)-1A, IL-1B, and IL-6) in all three BLBC cell lines but lower basal expression and minimal changes after *POLE1* suppression in LUBC cell lines (Figure S4G). Consistent with induction of a senescence-like phenotype, two BLBC cell lines (MDA-MB-231 and Hs578t) exhibited senescence-associated  $\beta$ -galactosidase (SA- $\beta$ -gal) activity, a common marker of replicative senescence, eight days after *POLE1* suppression (Figure 4F).

To temporally characterize the phenotypes induced by *POLE1* suppression, we stably transduced MDA-MB-231 cells with a DOX-inducible shRNA targeting *POLE1* and isolated two independent clones. Addition of DOX led to significant depletion of POLE after two days (Figures 4G and S4H). We observed pCHK1 induction concomitant with POLE depletion, and within a day, we observed accumulation of  $\gamma$ -H2AX and increases in the cytokine transcripts CSF3, IL-1A, IL-1B, and IL-6 (Figures 4G, 4H, and S4H). To test whether these viability effects are reversible, we treated cells with DOX for 0 to 6 days and then replated cells in the presence or absence of DOX. We observed that 3–4 days after DOX addition, coincident with the appearance of DNA damage markers, cells lose the ability to recover upon DOX withdrawal, consistent with irreversible changes (Figures 4I and S4I). Altogether, these data demonstrate that in BLBC, POLE loss leads to replication fork stalling followed by DNA damage, induction of a senescence-like phenotype, and irreversible loss of cell viability.

### ATR and CHK1 Kinase Activity Are Required for Resistance to POLE Suppression

Because we observe a differential requirement for POLE in BLBC cells compared with other breast cancer subtypes, we hypothesized that an intrinsic difference exists between these subtypes that drives sensitivity. BLBC tumors are suggested to have a BRCAness phenotype, signifying an intrinsic defect in DNA

(E) Output of GSEA analysis. Input is ranked Pearson correlation coefficient between gene expression in a given cell line and sensitivity of that cell line to POLE suppression. Green line, enrichment score along the ranked gene set. Dark lines, position of genes in the set within the ranked list. False discovery rate (FDR) values are indicated.

(F) Tumor xenograft volume for MDA-MB-231 cells expressing DOX-inducible shPOLE\_1 and shRNA-resistant POLE cDNA POLE (shPOLE Rescue) or VC (shPOLE VC). DOX in chow at day 0.  $n = 13$  on days 0–11,  $n = 8$  on days 12–18, representative of 3 independent experiments.

\* $p < 0.05$ , \*\* $p < 0.01$ , \*\*\* $p < 0.001$ , \*\*\*\* $p < 0.0001$ ; ns, not significant. Error bars are SEM.  $n \geq 3$  independent experiments. See also Figure S3 and Table S3.

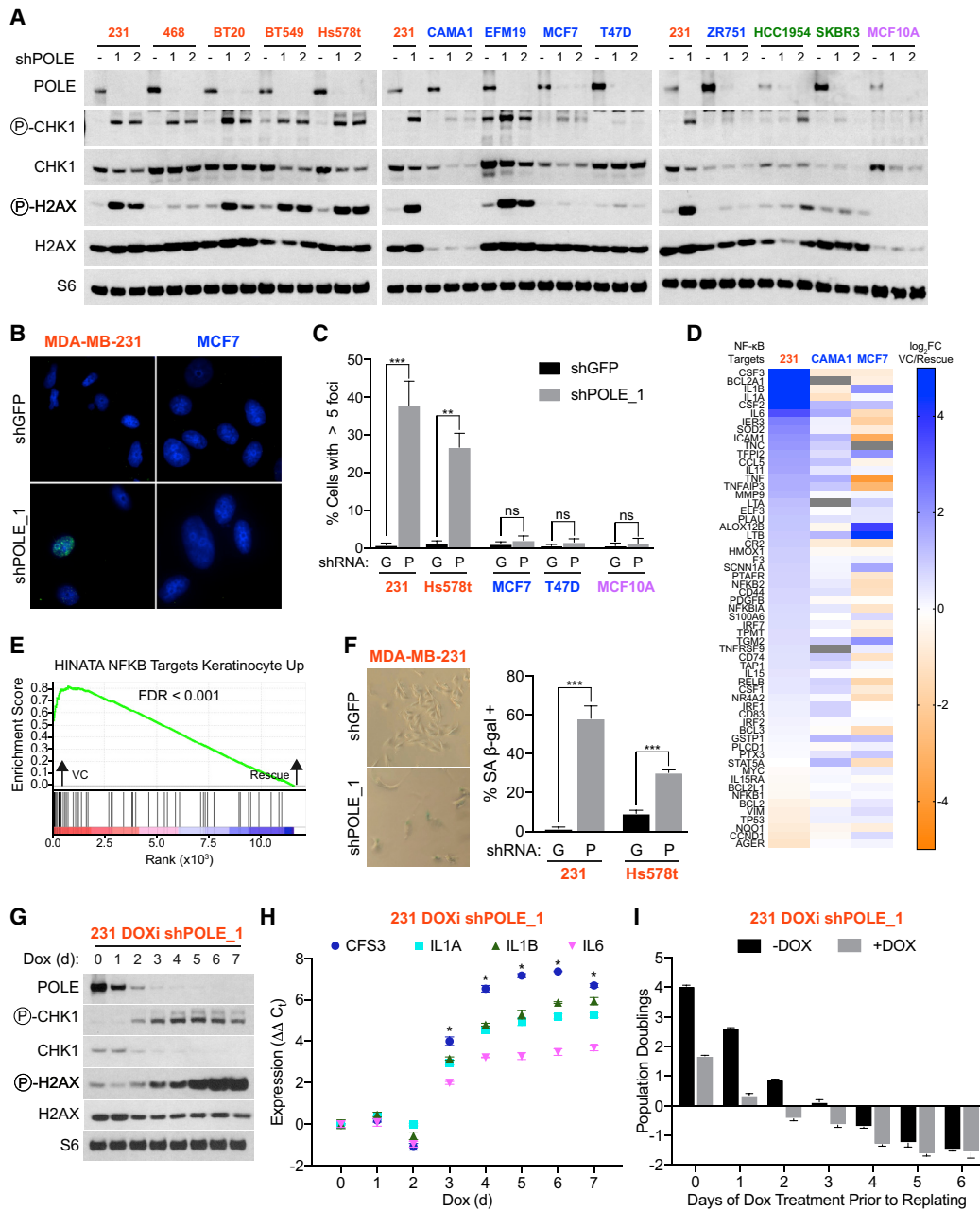


**Figure 4. POLE Suppression Leads to DNA Damage, Replication Fork Stalling, and Induction of Replicative Senescence in BLBC Cells**

(A) Immunoblots for the indicated proteins or modifications. Lysates from cell lines expressing shGFP (–) or shRNA targeting POLE (1, shPOLE\_1; 2, shPOLE\_2). CHK1 phosphorylation occurs at S345, and H2AX phosphorylation occurs at S139. Cell lines are grouped by classification: basal-like (orange), luminal (blue), Her2 amplified (HER2, green), or non-transformed (NT, purple).

(B and C) ssDNA assays. Representative immunofluorescence images (B) and quantification of BrdU-positive nuclei (C); BrdU (green) and DAPI (blue). Cells were infected with shRNAs (6 days), cultured with BrdU (10  $\mu$ M, last 4 days), and fixed.

(D) Heatmap reporting average  $\log_2$  fold change in gene expression (RNA sequencing [RNA-seq],  $n = 2$ ) for NF- $\kappa$ B target genes upon POLE suppression in indicated cell lines, relative to POLE cDNA rescue.

(E) Output of GSEA analysis. Input is the gene set ranked based on fold change upon POLE suppression in MDA-MB-231 cells relative to POLE cDNA rescue. The green line denotes the enrichment score along the ranked gene set. Dark lines denote locations of genes in the given gene set within this ranked list. FDR values are indicated.

(F) Senescence-associated  $\beta$ -galactosidase (SA- $\beta$ -gal) assay. Representative images (left) and quantification (right) of SA- $\beta$ -gal-positive cells from indicated cell lines 8 days after infection with shGFP or shPOLE\_1.

(legend continued on next page)

repair pathways in the absence of a *BRCA1* or *BRCA2* mutation (Lord and Ashworth, 2016).

To test whether inhibiting DNA damage response pathways would sensitize non-BLBC cells to POLE suppression, we treated MCF7 cells expressing either shGFP or shPOLE\_1 with inhibitors of three major DNA damage-sensing kinases (ATM, ATR, and DNA-PK) and measured viability. Inhibitors of ATM (KU55933) and DNA-PK (NU7441) equally affected viability in control and POLE-suppressed cells, whereas an ATR inhibitor (ATRi, AZD6738) synergized with POLE suppression in limiting viability of MCF7 and the non-transformed MCF10A cell line and hastened cell death in POLE-suppressed MDA-MB-231 cells (Figures S5A–S5E).

ATR is the central kinase regulator of the intra-S-phase checkpoint and becomes activated upon exposure of ssDNA structures such as those seen upon replication fork stalling. When activated, ATR acts to arrest cell-cycle progression and permit fork repair and restart primarily through its effector kinase CHK1 (Figure 5A) (Saldivar et al., 2017). Like ATR inhibition, treatment with a CHK1 inhibitor (CHK1i, MK8776) significantly reduced viability in POLE-suppressed MCF7 and MCF10A cells and hastened cell death in POLE-suppressed MDA-MB-231 cells (Figures S5F–S5H). We also observed synergy between ATRi or CHK1i and NFS1 suppression in both MCF7 and MCF10A cells, consistent with NFS1 supporting POLE function (Figures S5C, S5D, S5F, and S5G).

We next assessed effects on DNA damage of combined POLE or NFS1 suppression with ATRi or CHK1i treatment. Although drug treatment or suppression of POLE or NFS1 alone had minimal effects on DNA damage in MCF7 and MCF10A cells, combined inhibitor treatment with POLE or NFS1 suppression strongly induced  $\gamma$ -H2AX, similar to the fold induction observed in BLBC cell lines upon POLE suppression alone (Figure 5B). Cell-cycle profiling of POLE-suppressed MCF7 cells treated with ATRi or CHK1i for two days revealed a severe loss of EdU-incorporating cells (Figures 5C and 5D). Consistent with an irreversible arrest, removal of these inhibitors after two days and assessment of proliferation for three days showed that POLE-suppressed cells fail to recover from ATR or CHK1 inhibition, in contrast to control cells (Figure 5E). Most POLE-suppressed MCF7 cells treated with ATRi or CHK1i exhibited SA- $\beta$ -gal activity (Figures S5I and S5J). These data demonstrate that inhibition of the ATR/CHK1 pathway prevents cells from properly compensating for low levels of POLE.

### Hyperactive CDK2 Is Found in BLBC Tumors and Sensitizes Cells to POLE Suppression

We next asked why BLBC cells become sensitive to POLE suppression upon ATR and CHK1 inhibition. One critical effector of

CHK1 is the CDC25 family of phosphatases, which regulate G1/S, intra-S, and G2/M cell-cycle checkpoints by modulating CDK1/2 (Boutros et al., 2007). Given this pathway architecture, ATR/CHK1 engagement inhibits CDK1/2 activity (Figure 5A). Therefore, we considered whether BLBC tumors have hyperactive CDK1/2 activity. We consulted phosphoproteomic data obtained from primary breast tumor samples and observed hyperphosphorylation of phosphopeptides annotated to be either CDK1 or CDK2 targets in BLBC tumors compared with other breast cancer subtypes (Figures 6A, 6B, S6A, and S6B; Table S5). Interestingly, BLBC is known to harbor genetic alterations that affect CDK2 activity, such as p53 mutation, cyclin E overexpression, RB1 loss, and c-Myc amplification. These data implicate the genomic alterations intrinsic to BLBC in promoting a hyperactive CDK1/2 state.

We then inquired whether the synergistic effects of POLE suppression and ATRi or CHK inhibitor (CHKi) treatment depend on downstream activation of CDKs in non-BLBC cells. We used doses of CDK inhibitors expected to partially suppress activity of their targets without causing loss of cell viability or cell-cycle arrest. We observed that a CDK2 inhibitor (CDK2i, CDK2 inhibitor II) rescued cell viability upon combined inhibition of POLE and ATR or CHK1 (Figure S6C). In contrast, CDK1 inhibitor (CDK1i, RO-3306) or CDK4/6i (palbociclib) did not (Figure S6C). Upon combined inhibition of POLE and CHK1 in MCF7 cells,  $\gamma$ -H2AX induction was suppressed by compounds that can inhibit CDK2 (a second CDK2i, CVT-313, and a dual CDK1/2 inhibitor [CDK1/2i], CDK1/2 inhibitor III), but not by compounds that inhibit CDK1 or CDK4/6 (Figures 6C and S6D). Treatment with CDK2i also improved viability of BLBC cell line MDA-MB-231 upon DOX-induced POLE suppression and reduced DNA damage and pCHK1 (Figures S6E and S6F).

We then assessed whether the cell-cycle defects observed upon combined inhibition of POLE and ATR or CHK1 could be affected by CDK inhibitor treatment. CDK1/2i and CDK2i, but not CDK1i, prevented the loss of EdU+ cells after combined POLE and CHK1 inhibition in MCF7 cells (Figures 6D, 6E and S6G). The CDK1/2i and CDK2i conditions used did not block cell-cycle progression, suggesting that the conditions are used to fine-tune CDK2 activity toward homeostasis rather than blocking cell-cycle progression outright. We next treated MCF7 cells with combined inhibition of POLE and CHK1 and one of three CDK inhibitors for two days before removal of both drugs and assessment of proliferation. Combined treatment with CDK2i or CDK1/2i restored proliferation, whereas CDK1i did not (Figure 6F). These data support the hypothesis that CHK1i-mediated sensitization to POLE suppression is a result of effects on CDK2.

(G) Immunoblots for the indicated proteins or modifications of lysates derived from the MDA-MB-231 single-cell clone engineered to express DOX-inducible shPOLE\_1. DOX (0.5  $\mu$ g/mL) was added for the indicated number of days to induce POLE suppression before cell lysis. CHK1 phosphorylation occurs at S345, and H2AX phosphorylation occurs at S139.

(H) Representative relative expression ( $\Delta\Delta$ Ct) of indicated mRNAs (qPCR) before or upon addition of DOX (0.5  $\mu$ g/mL) for the indicated number of days. The asterisk indicates  $p < 0.05$  for cytokines on the indicated day relative to cytokine expression with no DOX.

(I) Representative replicative capacity of cells from (G) treated with DOX (0.5  $\mu$ g/mL) for the indicated number of days before replating in the absence (black bars) or presence (gray bars) of DOX, 5 days proliferation.

\* $p < 0.05$ , \*\* $p < 0.01$ , \*\*\* $p < 0.001$ , \*\*\*\* $p < 0.0001$ ; ns, not significant. Error bars are SEM.  $n \geq 3$  independent experiments unless otherwise noted. See also Figure S4 and Table S4.

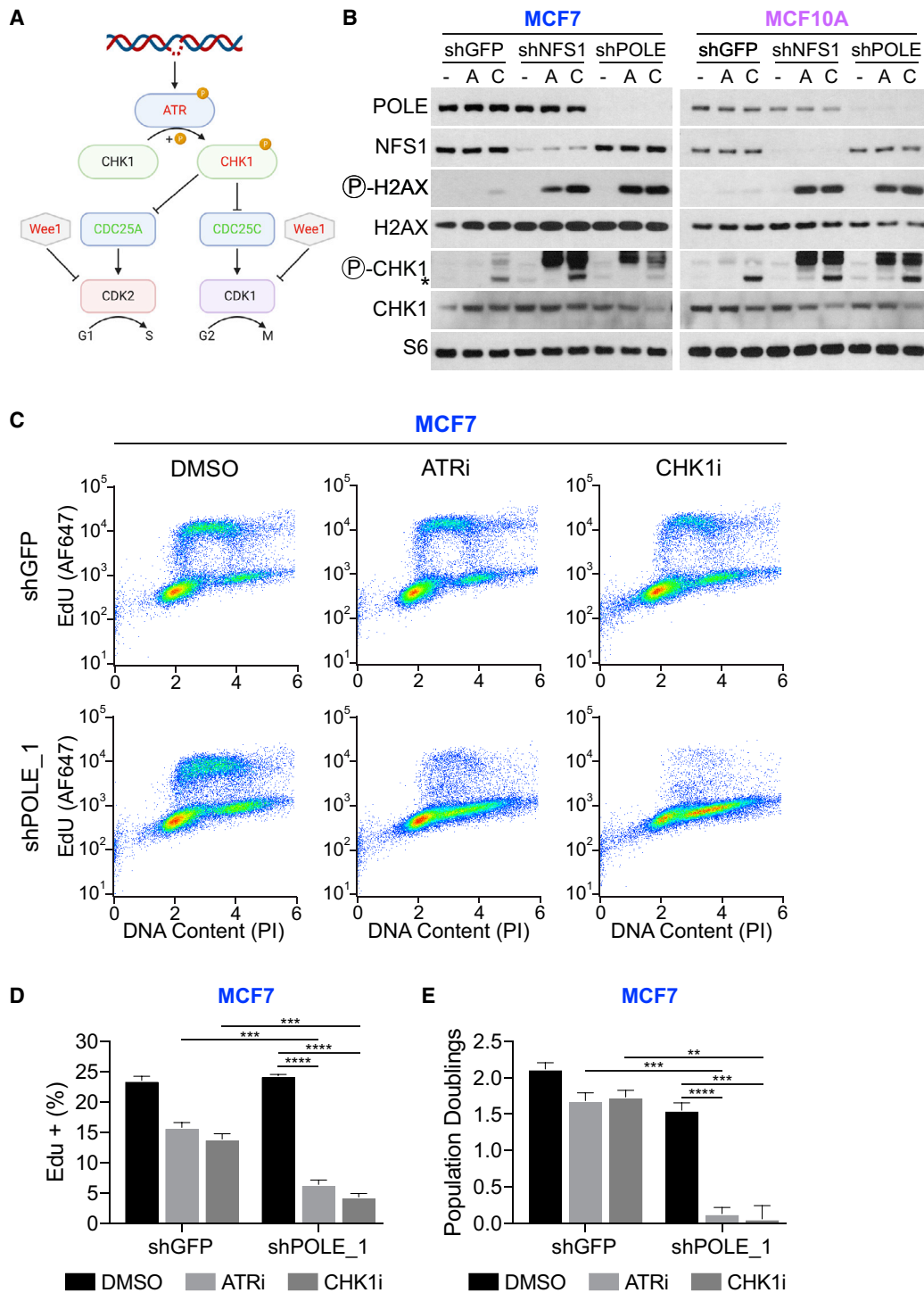


**Figure 5. ATR and CHK1 Kinase Activity Are Required for Resistance to POLE Suppression**

(A) Pathway outline. ATR senses replication stress and phosphorylates CHK1, resulting in its activation. CHK1 inhibits CDC25A and CDC25C, which remove inhibitory phosphorylation on CDK1/2 placed by Wee1. CDK2 promotes the G1-to-S transition, and CDK1 promotes the G2-to-M transition. Negative (red) and positive (green) regulators of CDK1/2 activity are indicated.

(B) Immunoblots for the indicated proteins or modifications. Lysates from MCF7 (luminal) or MCF10A (non-transformed) breast cells expressing shGFP, shNFS1, or shPOLE\_1 7 days after infection. Cells treated with vehicle (DMSO, -), 0.5  $\mu$ M Chk1 inhibitor MK8776 (C), or 0.5  $\mu$ M ATR inhibitor AZD6738 (A) 24 h before lysis. CHK1 phosphorylation occurs at S345, and H2AX phosphorylation occurs at S139. P-Chk1 blot; the asterisk indicates the predicted molecular weight of Chk1, and upper bands are consistent with ubiquitination.

(legend continued on next page)

CDK1/2 undergoes inhibitory phosphorylation by Wee1, an effect counteracted by the CDC25 phosphatases. We hypothesized that modulating this inhibitory phosphorylation on CDK2 would affect sensitivity to POLE suppression. Specifically, inhibition of Wee1 hyperactivates CDK1/2 and should induce sensitivity to POLE suppression. Similarly, suppression of CDC25A, which dephosphorylates CDK2, should counteract combined POLE and CHK1 inhibition, whereas suppression of CDC25C, which dephosphorylates CDK1, should not. Indeed, we observed a synthetic lethal interaction between NFS1 or POLE suppression and Wee1 inhibitor (Wee1i) AZD1775 in MCF7 and MCF10A cells (Figures S6H and S6I). CDK2i, but not CDK1i, rescued this induced sensitivity (Figure S6H). Similarly, combined Wee1i and POLE inhibition resulted in  $\gamma$ -H2AX induction and pCHK1 that was rescued with CDK2i, but not CDK1i (Figure 6G). Upon withdrawal of Wee1i, proliferative capacity did not recover in POLE-suppressed cells, consistent with induction of irreversible cell-cycle arrest (Figure 6H). Co-treatment of Wee1i and CDK2i, but not CDK1i, followed by drug removal restored proliferative capacity (Figure 6H). Similarly, suppression of CDK2 phosphatase CDC25A delayed DNA damage induced by combined POLE and CHK1 inhibition, whereas suppression of CDK1 phosphatase CDC25C did not (Figures S6J–S6L). Altogether, these data demonstrate that CDK2 is the downstream effector of the ATR/CHK1 pathway that mediates sensitivity to POLE suppression in LUBC (Figure 7).

## DISCUSSION

Here we identify POLE, the catalytic subunit of leading-strand DNA replicative polymerase Pol  $\epsilon$ , as a protein that drives sensitivity to ISC biosynthesis suppression in BLBC. Although all three major DNA polymerases, Pol  $\alpha$ , Pol  $\delta$ , and Pol  $\epsilon$ , coordinate an ISC (Stehling et al., 2013), our work supports a differential requirement only for POLE in BLBC and identifies the polymerase domain ISC-binding site in POLE as critical for maintaining viability in BLBC. Studies in *S. cerevisiae* propose a structural role for this ISC binding site and demonstrate that mutation of the site compromises polymerase activity because of loss of dNTP affinity. Consistent with these findings, we observe that NFS1 suppression affects replication by decreasing nucleotide incorporation and inducing cell-cycle defects and DNA damage, effects rescued by culturing cells in the ISC-protective condition of 3% O<sub>2</sub>.

POLE suppression similarly leads to marked cell proliferation defects and genomic instability in BLBC cell lines but with the added benefit of affecting established tumor growth because of O<sub>2</sub>-independent effects on proliferation. However, non-BLBC cell lines maintain viability at low POLE levels. In accordance, patients with genetic *POLE1* deficiency and mice with Pol  $\epsilon$  deficiency caused by deletion of accessory subunit Pole4 have only 5%–10% of WT POLE protein levels, yet patients sur-

vive to adulthood and outbred mice are viable (Bellelli et al., 2018; Logan et al., 2018; Pachlopnik Schmid et al., 2012). These models exhibit replication stress, delayed S-phase progression, and diminished replication origin activation with an accompanying increase in replication fork speed, phenotypes reminiscent of POLE suppression in LUBC cell lines. Similarly, *S. cerevisiae* strains lacking the polymerase and exonuclease domains of POLE maintain viability and have a prolonged S phase (Dua et al., 1999; Garbacz et al., 2018; Kesti et al., 1999). In these strains, Pol  $\delta$  performs both leading- and lagging-strand replication, imploring the question of whether Pol  $\delta$  mitigates effects of low POLE levels in higher-level organisms (Garbacz et al., 2018). These data indicate that most cell types have the capacity to maintain viability when POLE levels are low, yet BLBC cells have acquired sensitivity during tumorigenesis, suggesting that a therapeutic window may exist for the selective targeting of POLE in this subtype.

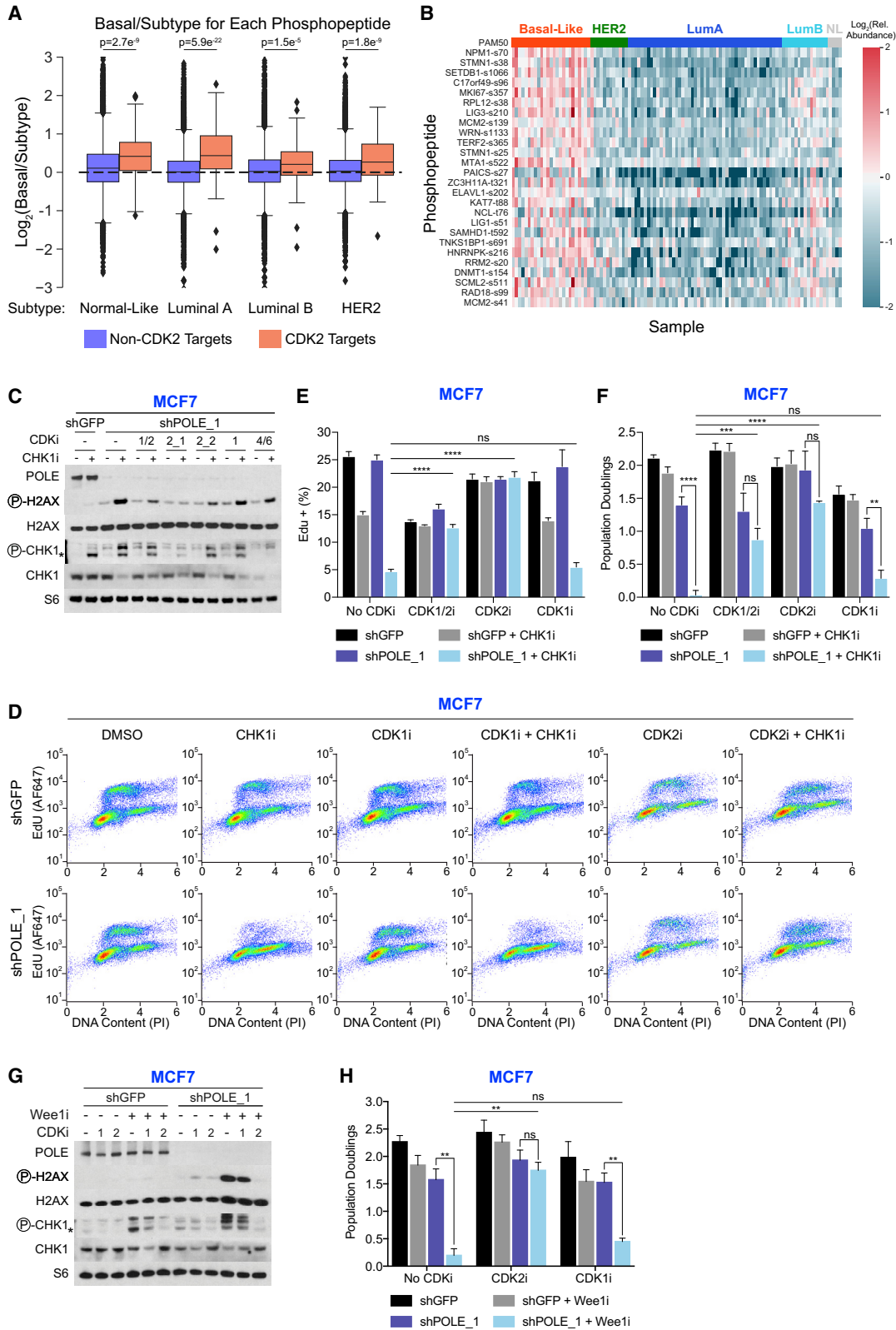
Compared with other subtypes, BLBC tumors exhibit elevated genomic instability stemming from *TP53* mutations, BRCA1 pathway dysfunction, c-Myc activation, cyclin E overexpression, and RB1 inactivation (Koboldt et al., 2012). Ashworth and colleagues described these tumors as having a BRCAness phenotype, signifying an intrinsic defect in DNA repair that mimics BRCA1 or BRCA2 loss (Lord and Ashworth, 2016). Additional roles for BRCA1/2 in replication fork protection led to the inclusion of defects in this pathway in the BRCAness definition (Byrum et al., 2019; Ray Chaudhuri et al., 2016; Schlacher et al., 2011, 2012). As such, inhibition of ATR and CHK1, central regulators of the intra-S checkpoint response to replication stress, is proposed to induce the BRCAness phenotype (Byrum et al., 2019). We find that cells that maintain viability upon POLE suppression are sensitized by treatment with ATRi or CHK1i, leading to phenotypes seen in BLBC upon POLE suppression alone. Indeed, genetic loss-of-function screens identify subunits of Pol  $\epsilon$  as synthetic liabilities with ATRi or CHK1i (Hustedt et al., 2019; Rogers et al., 2020; Wang et al., 2019). Our data and these genetic screens indicate that cells that maintain viability upon Pol  $\epsilon$  suppression depend on ATR/CHK1 for survival and that intrinsic BRCAness can sensitize to POLE suppression alone.

Many genetic changes that contribute to BRCAness in BLBC affect CDK2 (Figure 7). Compared with other subtypes, BLBC tumors also have increased expression of the CDK2 phosphatase CDC25A, but not CDK1 phosphatase CDC25C (Liu et al., 2018). Altogether, the genetic alterations in BLBC indicate hyperactive CDK2 function, a finding corroborated by our analysis of phosphoproteomic data from primary human breast tumors. We find that the CDK2 hyperactive state imposes a vulnerability to POLE suppression, because pharmacological or genetic inhibition of CDK2, but not CDK1, can rescue sensitivity to POLE suppression induced by treatment with ATRi, CHK1i, or Wee1i. These data support a model whereby intrinsic elevation of CDK2 activity in BLBC results in sensitivity to inhibition of

(C and D) Representative MCF7 cell-cycle profiles (C) and EdU-positive cell quantification (D) 8 days after infection and 48 h after the indicated drug treatment. Detection of incorporated EdU and DNA content (PI) by flow cytometry.

(E) Replicative capacity of MCF7 cells from (C) and (D) upon drug withdrawal, 3 days.

\*\* p < 0.01, \*\*\* p < 0.001, \*\*\*\* p < 0.0001. Error bars are SEM. n = 3 independent experiments. See also Figure S5.



(legend on next page)

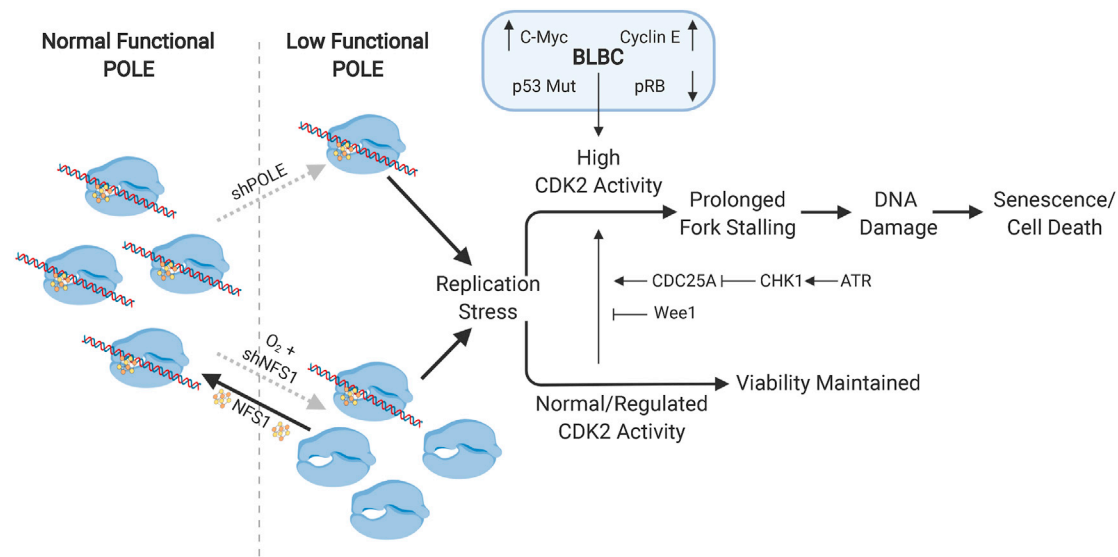


**Figure 7. Model of ISC Synthesis and POLE Disruption Affecting Breast Cancer Cells Dependent upon CDK2 Status**

Inhibition of ISC synthesis by NFS1 suppression in an elevated  $O_2$  environment reduces the pool of ISC-bound POLE, whereas POLE suppression reduces POLE protein levels. These perturbations reduce Pol  $\epsilon$  function and cause replication stress. Further effects depend on CDK2 status. Cells with a normal/regulated ATR/CHK1/CDC25A/CDK2 signaling axis maintain viability upon loss of functional POLE. However, cells with a hyperactive CDK2 experience prolonged replication fork stalling, DNA damage, induction of a senescence-like phenotype, and/or cell death. Mutations common to BLBC (p53 or pRB mutation, cyclin E, or c-Myc amplification) cause cells to enter the hyperactive CDK2 axis, whereas tumors with regulated CDK2 activity can be sensitized to low functional POLE levels by treatment with inhibitors of ATR, CHK1, or Wee1.

POLE-dependent functions (Figure 7). CDK2 activity has been implicated in the recruitment of helicase components to replication origins and in the firing of replication origins (Tanaka et al., 2007; Zegerman and Diffley, 2007). Elevated CDK2 activity may therefore create an increased dependence on replication proteins like POLE. Low levels of POLE could then uniquely create a two-pronged attack on these CDK2 hyperactive cells by inhibiting leading-strand replication and by potentially causing firing of origins with helicases but no accompanying polymerase. Indeed, POLE hypomorphic cells have altered stoichiometry of chromatin-bound POLE and CMG components (Bel-

lelli et al., 2018). Some combination of POLE's roles in leading-strand replication and origin firing likely contributes to increased sensitivity of its loss in CDK2 hyperactive cells.

Other tumor types with genomic alterations that affect CDK2 regulation may also exhibit this dependence. Included in this category are high-grade serous ovarian carcinomas, which have genomic alterations similar to BLBC, and LUBC tumors with acquired resistance to CDK4/6i therapy, which often exhibit altered CDK2 regulators, such as overexpression of cyclin E1 and loss of pRb (Koboldt et al., 2012). Such therapy-resistant LUBC tumors may also acquire vulnerabilities associated with

**Figure 6. Hyperactive CDK2 Is Found in BLBC Tumors and Sensitizes Cells to POLE Suppression**

(A) Boxplot reporting the relative abundance of phosphopeptides identified in human breast tumors. Basal-like tumors are compared with each breast cancer subtype.  $\log_2$  of the ratio is reported. Predicted CDK2 targets (orange) or not (blue) are grouped. Boxes denote population quartiles, whiskers are 0.9 and 0.1, and outlying points are marked.

(B) Heatmap reporting the relative abundance of predicted CDK2 target phosphopeptides significantly enriched in basal-like tumors versus other subtypes (FDR < 0.05). Samples are grouped by subtype (colored bar, top). The scale bar (right) indicates the  $\log_2$  peptide abundance relative to the mean. NL, normal-like.

(C) Immunoblots for the indicated proteins or modifications. Lysates from MCF7 cells expressing shGFP or shRNA targeting POLE (shPOLE\_1) 7 days after infection. Cells were treated with vehicle (-) or Chk1 inhibitor MK8776 (0.5  $\mu$ M, CHK1i), plus one of five inhibitors targeting CDKs, 24 h before harvest (1/2, CDK1/2 inhibitor III, 20 nM; 2\_1, CDK2 inhibitor II, 2  $\mu$ M; 2\_2, CDK2 inhibitor CVT-313, 2  $\mu$ M; 1, CDK1 inhibitor RO-3306, 1  $\mu$ M; 4/6, CDK4/6 inhibitor palbociclib, 250 nM). CHK1 phosphorylation occurs at S345, and H2AX phosphorylation occurs at S139. The asterisk on the pChk1 blot indicates the molecular weight of Chk1, and upper bands are consistent with ubiquitination.

(D and E) Representative MCF7 cell-cycle profiles (D) and quantification of EdU-positive cells (E) with 48 h treatment as in (C). Detection of incorporated EdU and DNA content (PI) by flow cytometry.

(F) Replicative capacity (3 days) of MCF7 cells infected with shGFP (gray bars) or shPOLE\_1 (blue bars) and treated as in (D) before drug withdrawal.

(G) Immunoblots as in (C). Cells were treated with vehicle (-) or Wee1 inhibitor AZD1775 (125 nM, Wee1i), plus inhibitors targeting CDK1/2, 24 h before harvest (1, RO-3306, 1  $\mu$ M; 2, CDK2 inhibitor II, 1  $\mu$ M).

(H) Replicative capacity (3 days) of MCF7 cells infected with shGFP (gray bars) or shPOLE\_1 (blue bars) and treated as in (D), including AZD1775 (250 nM, Wee1i) before drug withdrawal.

\*\*p < 0.01, \*\*\*p < 0.001, \*\*\*\*p < 0.0001; ns, not significant. Error bars are SEM. n  $\geq$  3 independent experiments. See also Figure S6 and Table S5.

CDK2 activation. Therefore, we propose that hyperactive CDK1/2 activity in BLBC or other tumor types may impose targetable liabilities for anti-cancer therapy and that these liabilities can be exploited by inhibition of POLE.

### STAR★METHODS

Detailed methods are provided in the online version of this paper and include the following:

- **KEY RESOURCES TABLE**
- **RESOURCE AVAILABILITY**
  - Lead Contact
  - Materials Availability
  - Data and Code Availability
- **EXPERIMENTAL MODEL AND SUBJECT DETAILS**
  - Animal Experiments
  - Cell Culture
- **METHOD DETAILS**
  - Animal Experiments
  - Generation of Recombinant Cell Lines
  - Proliferation Assays
  - Cell Cycle Analysis
  - Immunoblotting
  - Immunopurification
  - Aconitase Assay
  - Correlations of Publicly Available Data
  - Non-Denaturing BrdU Assay
  - DNA Fiber Assay
  - qPCR
  - Senescence Associated  $\beta$ -Galactosidase Assay
  - RNaseq
  - Phosphoproteomics Data Analysis
- **QUANTIFICATION AND STATISTICAL ANALYSIS**

### SUPPLEMENTAL INFORMATION

Supplemental Information can be found online at <https://doi.org/10.1016/j.molcel.2020.10.016>.

### ACKNOWLEDGMENTS

We thank Possemato lab members, Hannah L. Klein, and Mark R. Philips for comments; Michael Cammer and the Microscopy Laboratory; Varshini Vasudevaraja and the Applied Bioinformatics Laboratory; and the NYU Langone Genome Technology Center. Research was supported by NIH (T32GM007308, T32GM115313, CA228202, CA168940, GM132491, CA198543, CA168940, GM121994, P30CA016087, and R01ES025166) and Susan G. Komen for the Cure. R.P. is a scholar of the Pew Charitable Trusts and the Alexander and Margaret Stewart Trust, as well as an American Cancer Society Research Scholar. pCW57.1-MAT2A was a gift from David Sabatini. plentiCRISPR v2 was a gift from Feng Zhang.

### AUTHOR CONTRIBUTIONS

Conceptualization, R.P. and V.O.S.; Methodology, R.P. and V.O.S.; Investigation, V.O.S., E.G., T.R.K., N.H., S.W.A., E.M.T., E.K., G.C.W., S.S., S.A., H.M., B.G.N., T.T.H., and P.T.; Investigation – Phosphoproteomic Analysis, L.B. and K.V.R.; Writing – Original Draft, V.O.S.; Writing – Review & Editing, V.O.S. and R.P.; Funding Acquisition, Resources, and Supervision, R.P.

### DECLARATION OF INTERESTS

B.G.N. is cofounder of, holds equity in, and received consulting fees from Navire Pharmaceuticals and Northern Biologics, Inc. He receives consulting fees and has equity in Jengu Therapeutics. His spouse has equity in Mirati Therapeutics; Amgen, Inc.; Regeneron Pharmaceuticals; and Moderna Therapeutics. The other authors declare no competing interests.

Received: April 8, 2020

Revised: August 12, 2020

Accepted: October 9, 2020

Published: November 4, 2020

### REFERENCES

- Alvarez, S.W., Sviderskiy, V.O., Terzi, E.M., Papagiannakopoulos, T., Moreira, A.L., Adams, S., Sabatini, D.M., Birsoy, K., and Possemato, R. (2017). NFS1 undergoes positive selection in lung tumours and protects cells from ferroptosis. *Nature* 551, 639–643.
- Baranovskiy, A.G., Lada, A.G., Siebler, H.M., Zhang, Y., Pavlov, Y.I., and Tahirov, T.H. (2012). DNA polymerase  $\delta$  and  $\zeta$  switch by sharing accessory subunits of DNA polymerase  $\delta$ . *J. Biol. Chem.* 287, 17281–17287.
- Baranovskiy, A.G., Gu, J., Babayeva, N.D., Kurinov, I., Pavlov, Y.I., and Tahirov, T.H. (2017). Crystal structure of the human Pol $\epsilon$  B-subunit in complex with the C-terminal domain of the catalytic subunit. *J. Biol. Chem.* 292, 15717–15730.
- Beinert, H., Holm, R.H., and Münck, E. (1997). Iron-sulfur clusters: nature's modular, multipurpose structures. *Science* 277, 653–659.
- Bellelli, R., Borel, V., Logan, C., Svendsen, J., Cox, D.E., Nye, E., Metcalfe, K., O'Connell, S.M., Stamp, G., Flynn, H.R., et al. (2018). Pole Instability Drives Replication Stress, Abnormal Development, and Tumorigenesis. *Mol. Cell* 70, 707–721.
- Bertucci, F., Finetti, P., and Birnbaum, D. (2012). Basal breast cancer: a complex and deadly molecular subtype. *Curr. Mol. Med.* 12, 96–110.
- Birsoy, K., Possemato, R., Lorbeer, F.K., Bayraktar, E.C., Thiru, P., Yucel, B., Wang, T., Chen, W.W., Clish, C.B., and Sabatini, D.M. (2014). Metabolic determinants of cancer cell sensitivity to glucose limitation and biguanides. *Nature* 508, 108–112.
- Bolstad, B.M., Irizarry, R.A., Astrand, M., and Speed, T.P. (2003). A comparison of normalization methods for high density oligonucleotide array data based on variance and bias. *Bioinformatics* 19, 185–193.
- Bonferroni, C.E. (1936). Teoria statistica delle classi e calcolo delle probabilita (Libreria internazionale Seeber).
- Boutros, R., Lobo, V., and Ducommun, B. (2007). CDC25 phosphatases in cancer cells: key players? Good targets? *Nat. Rev. Cancer* 7, 495–507.
- Burgers, P.M.J., and Kunkel, T.A. (2017). Eukaryotic DNA Replication Fork. *Annu. Rev. Biochem.* 86, 417–438.
- Byrum, A.K., Vindigni, A., and Mosammaparast, N. (2019). Defining and Modulating 'BRCAness'. *Trends Cell Biol.* 29, 740–751.
- Chen, Y.H., Jones, M.J., Yin, Y., Crist, S.B., Colnaghi, L., Sims, R.J., 3rd, Rothenberg, E., Jallepalli, P.V., and Huang, T.T. (2015). ATR-mediated phosphorylation of FANCI regulates dormant origin firing in response to replication stress. *Mol. Cell* 58, 323–338.
- DeBerardinis, R.J., and Chandel, N.S. (2016). Fundamentals of cancer metabolism. *Sci. Adv.* 2, e1600200.
- Deshpande, A., Sicinski, P., and Hinds, P.W. (2005). Cyclins and cdks in development and cancer: a perspective. *Oncogene* 24, 2909–2915.
- Dua, R., Levy, D.L., and Campbell, J.L. (1999). Analysis of the essential functions of the C-terminal protein/protein interaction domain of *Saccharomyces cerevisiae* pol epsilon and its unexpected ability to support growth in the absence of the DNA polymerase domain. *J. Biol. Chem.* 274, 22283–22288.
- Garbacz, M.A., Lujan, S.A., Burkholder, A.B., Cox, P.B., Wu, Q., Zhou, Z.-X., Haber, J.E., and Kunkel, T.A. (2018). Evidence that DNA polymerase

- $\delta$  contributes to initiating leading strand DNA replication in *Saccharomyces cerevisiae*. *Nat. Commun.* 9, 858.
- Gari, K., León Ortiz, A.M., Borel, V., Flynn, H., Skehel, J.M., and Boulton, S.J. (2012). MMS19 links cytoplasmic iron-sulfur cluster assembly to DNA metabolism. *Science* 337, 243–245.
- Hanahan, D., and Weinberg, R.A. (2011). Hallmarks of cancer: the next generation. *Cell* 144, 646–674.
- Hornbeck, P.V., Kornhauser, J.M., Tkachev, S., Zhang, B., Skrzypek, E., Murray, B., Latham, V., and Sullivan, M. (2012). PhosphoSitePlus: a comprehensive resource for investigating the structure and function of experimentally determined post-translational modifications in man and mouse. *Nucleic Acids Res.* 40, D261–D270.
- Hunter, J.D. (2007). Matplotlib: A 2D graphics environment. *Comput. Sci. Eng.* 9, 90–95.
- Hustedt, N., Álvarez-Quiñón, A., McEwan, A., Yuan, J.Y., Cho, T., Koob, L., Hart, T., and Durocher, D. (2019). A consensus set of genetic vulnerabilities to ATR inhibition. *Open Biol.* 9, 190156.
- Jain, R., Vanamee, E.S., Dzikovski, B.G., Buku, A., Johnson, R.E., Prakash, L., Prakash, S., and Aggarwal, A.K. (2014). An iron-sulfur cluster in the polymerase domain of yeast DNA polymerase  $\epsilon$ . *J. Mol. Biol.* 426, 301–308.
- Kesti, T., Flick, K., Keränen, S., Syväoja, J.E., and Wittenberg, C. (1999). DNA polymerase epsilon catalytic domains are dispensable for DNA replication, DNA repair, and cell viability. *Mol. Cell* 3, 679–685.
- Koboldt, D.C., Fulton, R.S., McLellan, M.D., Schmidt, H., Kalicki-Verizer, J., McMichael, J.F., Fulton, L.L., Dooling, D.J., Ding, L., Mardis, E.R., et al.; Cancer Genome Atlas Network (2012). Comprehensive molecular portraits of human breast tumours. *Nature* 490, 61–70.
- Liu, J.C., Granieri, L., Shrestha, M., Wang, D.Y., Vorobieva, I., Rubie, E.A., Jones, R., Ju, Y., Pellecchia, G., Jiang, Z., et al. (2018). Identification of CDC25 as a Common Therapeutic Target for Triple-Negative Breast Cancer. *Cell Rep.* 23, 112–126.
- Logan, C.V., Murray, J.E., Parry, D.A., Robertson, A., Bellelli, R., Tarnauskaitė, Ž., Challis, R., Cleal, L., Borel, V., Fluteau, A., et al.; SGP Consortium (2018). DNA Polymerase Epsilon Deficiency Causes IMAGE Syndrome with Variable Immunodeficiency. *Am. J. Hum. Genet.* 103, 1038–1044.
- Lord, C.J., and Ashworth, A. (2012). The DNA damage response and cancer therapy. *Nature* 481, 287–294.
- Lord, C.J., and Ashworth, A. (2016). BRCAness revisited. *Nat. Rev. Cancer* 16, 110–120.
- Lord, C.J., and Ashworth, A. (2017). PARP inhibitors: Synthetic lethality in the clinic. *Science* 355, 1152–1158.
- Maio, N., and Rouault, T.A. (2015). Iron-sulfur cluster biogenesis in mammalian cells: New insights into the molecular mechanisms of cluster delivery. *Biochim. Biophys. Acta* 1853, 1493–1512.
- Marcotte, R., Sayad, A., Brown, K.R., Sanchez-Garcia, F., Reimand, J., Haider, M., Virtanen, C., Bradner, J.E., Bader, G.D., Mills, G.B., et al. (2016). Functional Genomic Landscape of Human Breast Cancer Drivers, Vulnerabilities, and Resistance. *Cell* 164, 293–309.
- McKinney, W. (2010). Data structures for statistical computing in python. In Proceedings of the 9th Python in Science Conference, pp. 51–56, Austin, TX.
- Morgan, D.O. (1997). Cyclin-dependent kinases: engines, clocks, and microprocessors. *Annu. Rev. Cell Dev. Biol.* 13, 261–291.
- Mukherjee, B., Tomimatsu, N., and Burma, S. (2015). Immunofluorescence-based methods to monitor DNA end resection. *Methods Mol. Biol.* 1292, 67–75.
- Netz, D.J., Stith, C.M., Stümpfig, M., Köpf, G., Vogel, D., Genau, H.M., Stodola, J.L., Lill, R., Burgers, P.M., and Pierik, A.J. (2011). Eukaryotic DNA polymerases require an iron-sulfur cluster for the formation of active complexes. *Nat. Chem. Biol.* 8, 125–132.
- Netz, D.J., Mascarenhas, J., Stehling, O., Pierik, A.J., and Lill, R. (2014). Maturation of cytosolic and nuclear iron-sulfur proteins. *Trends Cell Biol.* 24, 303–312.
- Oliphant, T.E. (2006). A guide to NumPy, *Volume 1* (Trelgol Publishing USA).
- Otto, T., and Scisinski, P. (2017). Cell cycle proteins as promising targets in cancer therapy. *Nat. Rev. Cancer* 17, 93–115.
- Pachlopnik Schmid, J., Lemoine, R., Nehme, N., Cormier-Daire, V., Revy, P., Debeurme, F., Debré, M., Nitschke, P., Bole-Feysot, C., Legeai-Mallet, L., et al. (2012). Polymerase  $\epsilon$ 1 mutation in a human syndrome with facial dysmorphism, immunodeficiency, livedo, and short stature (“FILS syndrome”). *J. Exp. Med.* 209, 2323–2330.
- Paul, V.D., and Lill, R. (2015). Biogenesis of cytosolic and nuclear iron-sulfur proteins and their role in genome stability. *Biochim. Biophys. Acta* 1853, 1528–1539.
- Ray Chaudhuri, A., Callen, E., Ding, X., Gogola, E., Duarte, A.A., Lee, J.E., Wong, N., Lafarga, V., Calvo, J.A., Panzarino, N.J., et al. (2016). Replication fork stability confers chemoresistance in BRCA-deficient cells. *Nature* 535, 382–387.
- Rimawi, M.F., Schiff, R., and Osborne, C.K. (2015). Targeting HER2 for the treatment of breast cancer. *Annu. Rev. Med.* 66, 111–128.
- Rogers, R.F., Walton, M.I., Cherry, D.L., Collins, I., Clarke, P.A., Garrett, M.D., and Workman, P. (2020). CHK1 inhibition is synthetically lethal with loss of B-family DNA polymerase function in human lung and colorectal cancer cells. *Cancer Res.* 80, 1735–1747.
- Saldívar, J.C., Cortez, D., and Cimprich, K.A. (2017). The essential kinase ATR: ensuring faithful duplication of a challenging genome. *Nat. Rev. Mol. Cell Biol.* 18, 622–636.
- Schlacher, K., Christ, N., Siaud, N., Egashira, A., Wu, H., and Jasin, M. (2011). Double-strand break repair-independent role for BRCA2 in blocking stalled replication fork degradation by MRE11. *Cell* 145, 529–542.
- Schlacher, K., Wu, H., and Jasin, M. (2012). A distinct replication fork protection pathway connects Fanconi anemia tumor suppressors to RAD51-BRCA1/2. *Cancer Cell* 22, 106–116.
- Seabold, S., and Perktold, J. (2010). Statsmodels: Econometric and statistical modeling with Python. In Proceedings of the 9th Python in Science Conference, pp. 92–96, Austin, TX.
- Sengupta, S., van Deursen, F., de Piccoli, G., and Labib, K. (2013). Dpb2 integrates the leading-strand DNA polymerase into the eukaryotic replisome. *Curr. Biol.* 23, 543–552.
- Siegel, R.L., Miller, K.D., and Jemal, A. (2016). Cancer statistics, 2016. *CA Cancer J. Clin.* 66, 7–30.
- Stehling, O., Vashisht, A.A., Mascarenhas, J., Jonsson, Z.O., Sharma, T., Netz, D.J., Pierik, A.J., Wohlschlegel, J.A., and Lill, R. (2012). MMS19 assembles iron-sulfur proteins required for DNA metabolism and genomic integrity. *Science* 337, 195–199.
- Stehling, O., Mascarenhas, J., Vashisht, A.A., Sheftel, A.D., Niggemeyer, B., Rösser, R., Pierik, A.J., Wohlschlegel, J.A., and Lill, R. (2013). Human CIA2A-FAM96A and CIA2B-FAM96B integrate iron homeostasis and maturation of different subsets of cytosolic-nuclear iron-sulfur proteins. *Cell Metab.* 18, 187–198.
- Stehling, O., Wilbrecht, C., and Lill, R. (2014). Mitochondrial iron-sulfur protein biogenesis and human disease. *Biochimie* 100, 61–77.
- Subramanian, A., Tamayo, P., Mootha, V.K., Mukherjee, S., Ebert, B.L., Gillette, M.A., Paulovich, A., Pomeroy, S.L., Golub, T.R., Lander, E.S., and Mesirov, J.P. (2005). Gene set enrichment analysis: a knowledge-based approach for interpreting genome-wide expression profiles. *Proc. Natl. Acad. Sci. USA* 102, 15545–15550.
- Tanaka, S., Umemori, T., Hirai, K., Muramatsu, S., Kamimura, Y., and Araki, H. (2007). CDK-dependent phosphorylation of Sld2 and Sld3 initiates DNA replication in budding yeast. *Nature* 445, 328–332.
- Ter Beek, J., Parkash, V., Bylund, G.O., Osterman, P., Sauer-Eriksson, A.E., and Johansson, E. (2019). Structural evidence for an essential Fe-S cluster in the catalytic core domain of DNA polymerase  $\epsilon$ . *Nucleic Acids Res.* 47, 5712–5722.

- Tsherniak, A., Vazquez, F., Montgomery, P.G., Weir, B.A., Kryukov, G., Cowley, G.S., Gill, S., Harrington, W.F., Pantel, S., Krill-Burger, J.M., et al. (2017). Defining a Cancer Dependency Map. *Cell* **170**, 564–576.
- Turner, N.C., Slamon, D.J., Ro, J., Bondarenko, I., Im, S.-A., Masuda, N., Colleoni, M., DeMichele, A., Loi, S., Verma, S., et al. (2018). Overall Survival with Palbociclib and Fulvestrant in Advanced Breast Cancer. *N. Engl. J. Med.* **379**, 1926–1936.
- van der Walt, S., Colbert, S.C., and Varoquaux, G. (2011). The NumPy array: a structure for efficient numerical computation. *Comput. Sci. Eng.* **13**, 22–30.
- Vander Heiden, M.G., and DeBerardinis, R.J. (2017). Understanding the Intersections between Metabolism and Cancer Biology. *Cell* **168**, 657–669.
- Veatch, J.R., McMurray, M.A., Nelson, Z.W., and Gottschling, D.E. (2009). Mitochondrial dysfunction leads to nuclear genome instability via an iron-sulfur cluster defect. *Cell* **137**, 1247–1258.
- Virtanen, P., Gommers, R., Oliphant, T.E., Haberland, M., Reddy, T., Cournapeau, D., Burovski, E., Peterson, P., Weckesser, W., Bright, J., et al.; SciPy 1.0 Contributors (2020). SciPy 1.0: fundamental algorithms for scientific computing in Python. *Nat. Methods* **17**, 261–272.
- Wang, C., Wang, G., Feng, X., Shepherd, P., Zhang, J., Tang, M., Chen, Z., Srivastava, M., McLaughlin, M.E., Navone, N.M., et al. (2019). Genome-wide CRISPR screens reveal synthetic lethality of RNASEH2 deficiency and ATR inhibition. *Oncogene* **38**, 2451–2463.
- Waskom, M., Botvinnik, O., O’Kane, D., Hobson, P., Lukauskas, S., Gemperline, D.C., and Augspurger, T. (2017). Seaborn. July. <https://zenodo.org/record/824567>.
- Zegerman, P., and Diffley, J.F. (2007). Phosphorylation of Sld2 and Sld3 by cyclin-dependent kinases promotes DNA replication in budding yeast. *Nature* **445**, 281–285.
- Zeman, M.K., and Cimprich, K.A. (2014). Causes and consequences of replication stress. *Nat. Cell Biol.* **16**, 2–9.

STAR★METHODS

KEY RESOURCES TABLE

REAGENT or RESOURCE	SOURCE	IDENTIFIER
<b>Antibodies</b>		
HRP-linked anti-mouse	Santa Cruz	Cat# sc-2066; RRID:AB_631757
HRP-linked anti-rabbit	Santa Cruz	Cat# sc-2054; RRID:AB_631748
$\beta$ -actin	Cell Signaling Tech.	Cat# 8457; RRID:AB_10950489
NFS-1	Cell Signaling Tech.	Cat# sc-365308; RRID:AB_10843245
FECH	Cell Signaling Tech.	sc-377377
CDC25C	Cell Signaling Tech.	Cat# sc-13138; RRID:AB_627227
CHK1	Cell Signaling Tech.	Cat# sc-8408; RRID:AB_627257
POLE	GeneTex	GTX132100
RPS6	Cell Signaling Tech.	Cat# 2217; RRID:AB_331355
TFRC	Cell Signaling Tech.	Cat# 13208; RRID:AB_2798150
FTH1	Cell Signaling Tech.	Cat# 3998; RRID:AB_1903974
$\gamma$ -H2AX	Cell Signaling Tech.	Cat# 9718; RRID:AB_2118009
H2AX	Cell Signaling Tech.	Cat# 2595; RRID:AB_10694556
Phospho-Chk1 S345	Cell Signaling Tech.	Cat# 2348; RRID:AB_331212
HA	Cell Signaling Tech.	Cat# 2367; RRID:AB_10691311
POLD	Abcam	ab186407
POLA	Abcam	Cat# ab31777; RRID:AB_731976
BrdU/CldU	Abcam	Cat# ab6326; RRID:AB_305426
BrdU/IdU	BD Biosciences	Cat# 347580; RRID:AB_10015219
Goat Anti-Rat IgG H&L, Alexa Fluor 594	Abcam	Cat# ab150160; RRID:AB_2756445
Anti-Mouse IgG, Alexa Fluor 488	Cell Signaling Tech.	Cat# 4410; RRID:AB_1904023
FLAG	Sigma	Cat# F1804; RRID:AB_262044
<b>Chemicals, Peptides, and Recombinant Proteins</b>		
Matrigel	Corning	356234
RPMI	Corning	10-040
PrimeSTAR DNA polymerase	Takara	R040A
X-Gal	Crystalgen Inc.	AG0428
Doxycycline hyclate	Fisher Scientific	AAJ6057914
Potassium Hexacyanoferrate (II)	Sigma	P9387
Potassium Hexacyanoferrate (III)	Sigma	P8131
Sodium Phosphate Dibasic	Sigma	S5136
Sodium Phosphate Monobasic	Sigma	S5011
Hydroxyurea	Sigma	H8627
Methyl Methanesulfonate	Sigma	129925
5-Iodo-2'-deoxyuridine	Sigma	I7125
5-Chloro-2'-deoxyuridine	Sigma	C6891
Ammonium Hydroxide solution	Sigma	338818
Sodium Formate	Sigma	71539
DAPI	Sigma	D9542
5-Bromo-2'-Deoxyuridine	Sigma	B5002
Hydrocortisone	Sigma	H0888
Cholera toxin	Sigma	C8052
Insulin	Sigma	I0516

(Continued on next page)

**Continued**

REAGENT or RESOURCE	SOURCE	IDENTIFIER
PhosSTOP	Sigma	4906845001
MK-1775	Cayman Chemical	21266
RO-3306	Cayman Chemical	15149
PD-0332991	Cayman Chemical	16273
Cdk2 inhibitor II	Cayman Chemical	15154
MK-8776	SelleckChem	S2765
KU-55933	SelleckChem	S1092
NU7441	SelleckChem	S2638
AZD6738	SelleckChem	S7693
PVDF Membrane	Millipore	IPVH00010
Quick Ligase	New England Biolabs	M2200
Fetal Bovine Serum	Peak Serum	N/A
CDK1/2 Inhibitor III	Fisher Scientific	2177141MG
Superscript IV	Invitrogen	18090010
Polyethylenimine	Polysciences	239662
EGF	Life Technologies	PHG0311L
Puromycin	Sigma	P7255
Blasticidin	ThermoFisher	R21001
Sodium Pyruvate	Life Technologies	11360070
Uridine	Sigma	U3003
Hypoxanthine	Sigma	H9377
Bolt 4–12% Bis-Tris polyacrylamide gels	Life Technologies	NW04125
3–8% Tris-Acetate polyacrylamide gels	Life Technologies	EA03785BOX
Protein G Sepharose	Sigma	P3296
3X-FLAG peptide	Sigma	F4799
RNase OUT	Invitrogen	10777019
Maxima qPCR master mix	ThermoFisher	K0222
<b>Critical Commercial Assays</b>		
Aconitase Assay Kit	Sigma	MAK051
Click-iT Plus EdU Alexa Fluor 647 Flow Cytometry Assay Kit	ThermoFisher	C10634
CellTiter-Glo	Promega	G7570
Pierce BCA Protein Assay	Fisher Scientific	23225
RNeasy Plus Mini Kit	QIAGEN	74136
Qiaprep Spin Miniprep Kit	QIAGEN	27106
QIAquick Gel Extraction Kit	QIAGEN	28706
<b>Deposited Data</b>		
RNaseq Data Supporting <a href="#">Figures 4D, S4D, and S4E</a> and <a href="#">Table S4</a>	This paper	GEO: GSE159052
Primary Data	This paper	Mendeley Data: <a href="https://doi.org/10.17632/xvgb9rg7b7.1">https://doi.org/10.17632/xvgb9rg7b7.1</a>
<b>Experimental Models: Cell Lines</b>		
MDA-MB-231	ATCC	N/A
MDA-MB-468	ATCC	N/A
BT-20	ATCC	N/A
BT-549	ATCC	N/A
Hs578t	ATCC	N/A
MCF7	ATCC	N/A

(Continued on next page)

**Continued**

REAGENT or RESOURCE	SOURCE	IDENTIFIER
T47D	ATCC	N/A
CAMA-1	ATCC	N/A
ZR-75-1	ATCC	N/A
SK-BR-3	ATCC	N/A
HCC1954	ATCC	N/A
MCF10A	ATCC	N/A
EFM-19	DSMZ	N/A
293FT	Broad Institute	N/A
Experimental Models: Organisms/Strains		
NOD.CB17-Prkdcscid/J	Jackson Labs	001303
Oligonucleotides		
DNA primers	This Study	See <a href="#">Table S1</a>
Recombinant DNA		
pLKO.1P shGFP	The RNAi Consortium	TRCN0000072203
pLKO.1P shRFP	The RNAi Consortium	TRCN0000072186
pLKO.1P shNFS1_1	<a href="#">Alvarez et al., 2017</a>	Addgene 102963
pLKO.1P shNFS1_2	<a href="#">Alvarez et al., 2017</a>	Addgene 102964
pLKO.1P shNFS1_3	<a href="#">Alvarez et al., 2017</a>	Addgene 102966
pLKO.1P POLE1_1, TRCN0000052973	This Study	Addgene 160762
pLKO.1B POLE1_1	This Study	Addgene 160763
pLKO.1P POLE1_2, TRCN0000052975	This Study	Addgene 160764
pLKO.1B POLE1_2	This Study	Addgene 160765
pLKO.1P POLE2, TRCN0000052984	This Study	Addgene 160766
pLKO.1P CDC25A_1, TRCN0000002430	This Study	Addgene 160767
pLKO.1P CDC25A_2, TRCN0000238780	This Study	Addgene 160768
pLKO.1P CDC25C_1, TRCN0000002432	This Study	Addgene 160769
pLKO.1P CDC25C_2, TRCN0000314866	This Study	Addgene 160770
pLKO.1P BRIP1_1, TRCN0000049914	This Study	Addgene 160771
pLKO.1P BRIP1_2, TRCN0000049916	This Study	Addgene 160772
pLKO.1P CISD1_1, TRCN0000278357	This Study	Addgene 160773
pLKO.1P CISD1_2, TRCN0000278404	This Study	Addgene 160774
pLKO.1P CISD2_1, TRCN0000239665	This Study	Addgene 160775
pLKO.1P CISD2_2, TRCN0000239663	This Study	Addgene 160776
pLKO.1P DDX11_1, TRCN0000152654	This Study	Addgene 160777
pLKO.1P DDX11_2, TRCN0000156039	This Study	Addgene 160778
pLKO.1P DNA2_1, TRCN0000009830	This Study	Addgene 160779
pLKO.1P DNA2_2, TRCN0000039921	This Study	Addgene 160780
pLKO.1P ERCC2_1, TRCN0000285423	This Study	Addgene 160781
pLKO.1P ERCC2_2, TRCN0000275618	This Study	Addgene 160782
pLKO.1P EXO5_1, TRCN0000138174	This Study	Addgene 160783
pLKO.1P EXO5_2, TRCN0000135486	This Study	Addgene 160784
pLKO.1P MUTYH_1, TRCN0000333169	This Study	Addgene 160785
pLKO.1P MUTYH_2, TRCN0000333170	This Study	Addgene 160786
pLKO.1P NTHL1_1, TRCN0000007915	This Study	Addgene 160787
pLKO.1P NTHL1_2, TRCN0000007916	This Study	Addgene 160788
pLKO.1P POLA1_1, TRCN0000298738	This Study	Addgene 160789
pLKO.1P POLA1_2, TRCN0000331115	This Study	Addgene 160790
pLKO.1P POLD1_1, TRCN0000342684	This Study	Addgene 160791

(Continued on next page)

**Continued**

REAGENT or RESOURCE	SOURCE	IDENTIFIER
pLKO.1P POLD1_2, TRCN0000352782	This Study	Addgene 160792
pLKO.1P PPAT_1, TRCN0000304118	This Study	Addgene 160793
pLKO.1P PPAT_2, TRCN0000300653	This Study	Addgene 160794
pLKO.1P PRIM2_1, TRCN0000000199	This Study	Addgene 160795
pLKO.1P PRIM2_2, TRCN0000000201	This Study	Addgene 160796
pLKO.1P REV3L_1, TRCN0000053127	This Study	Addgene 160797
pLKO.1P REV3L_2, TRCN0000244438	This Study	Addgene 160798
pLKO.1P RTEL1_1, TRCN0000051669	This Study	Addgene 160799
pLKO.1P RTEL1_2, TRCN0000051672	This Study	Addgene 160800
pCW57.1-MAT2A	Addgene	Addgene 100512
pCW57.1 DOX off blast NFS1	This Study	Addgene 160801
pMXS-IRES-Blast	Cell Biolabs	RTV-016
pMXS-IRES-Blast POLE1	This Study	Addgene 160802
pMXS-IRES-Blast POLE1 N-ISCmut	This Study	Addgene 160803
pMXS-IRES-Blast POLE1 C-ISCmut	This Study	Addgene 160804
pMXS-IRES-Blast POLD1	This Study	Addgene 160805
pMXS-IRES-Blast POLD1 ISCmut	This Study	Addgene 160806
pMXS-IRES-Blast POLA1	This Study	Addgene 160807
pMXS-IRES-Blast POLA1 ISCmut	This Study	Addgene 160808
pMXS-IRES-Blast HA-POLE2	This Study	Addgene 160809
Tet-pLKO-puro shPOLE1_1	This Study	Addgene 160810
pLENTICRISPR sgNFS1	<a href="#">Alvarez et al., 2017</a>	Addgene 102979
Software and Algorithms		
FlowJo V.10	N/A	N/A
Other		
Z2 Coulter Counter	Beckman	Model Z2
Hypoxic Incubator	ThermoFisher	HeraCell 150i
Attune NxT Flow Cytometer	ThermoFisher	N/A

**RESOURCE AVAILABILITY**

**Lead Contact**

Further information and requests for resources and reagents should be directed to and will be fulfilled by the Lead Contact, Richard Possemato ([Richard.Possemato@nyulangone.org](mailto:Richard.Possemato@nyulangone.org)).

**Materials Availability**

Plasmids novel to this study and corresponding sequences have been deposited at Addgene (<http://www.addgene.org/>).

**Data and Code Availability**

Primary RNaseq data available at GEO: GSE159052 (<https://www.ncbi.nlm.nih.gov/geo/>). Other primary data have been uploaded to Mendeley Data: <https://doi.org/10.17632/xvgb9rg7b7.1>.

**EXPERIMENTAL MODEL AND SUBJECT DETAILS**

**Animal Experiments**

Xenograft mammary tumor experiments used 4–8 week old female NOD.CB17 Scid/J mice (Jackson Labs). All experiments involving mice were carried out with approval from the Committee for Animal Care and under supervision of the Division of Comparative Medicine at NYU Langone Medical Center.

### Cell Culture

Cell lines were tested to be mycoplasma free by PCR based methods and authenticity verified by STR profiling (Duke University). Cells were cultured in RPMI supplemented with 10% IFS (Sigma) and penicillin/streptomycin except MCF10A cells, which were cultured in DMEM/F12 media containing 5% horse serum, 1% penicillin/streptomycin, 20ng/mL EGF, 500ng/mL hydrocortisone, 100ng/mL Cholera toxin, 10 $\mu$ g/mL insulin. O<sub>2</sub> concentration was controlled by placing cells in a hypoxic incubator (HeraCell 150i, Thermo Fisher). Cells were placed at indicated O<sub>2</sub> concentration following infection.

### METHOD DETAILS

#### Animal Experiments

Tumors were initiated into 4-8 week old female NOD.CB17 Scid/J mice orthotopically in the mouse mammary gland by implanting 500,000 cells in 33% matrigel into the 4<sup>th</sup> murine mammary fat pad in a total volume of 25  $\mu$ L. Expression of shPOLE\_1 was induced by switching mice onto doxycycline chow (600 mg/kg) upon formation of palpable tumors. Tumor Volume was assessed using caliper measurements and volume was calculated using  $(L \cdot W^2)/2$ .

#### Generation of Recombinant Cell Lines

Lentiviral constructs were transfected with lentiviral packaging vectors  $\Delta$ VPR and CMV VSV-G, while retroviral constructs were transfected with pCL-Ampho into HEK293 cells using polyethylenimine. Media was changed 12-16 hours post infection, and virus was collected 48 and 72 hours post infection and combined. Virus was passed through a 0.45  $\mu$ m filter and stored at  $-80^\circ\text{C}$  or used immediately. One day prior to infection, cells were plated into 6-well tissue culture plates. Cells were infected with virus in media containing 1  $\mu$ g/ml polybrene via spin infection in a Beckman Coulter Allegra X-12R centrifuge with an SX4750 rotor and Microplate Carrier attachment at 2,250 rpm for 30 min. A multiplicity of infection of 2.5 was used for all shNFS1 experiments and a multiplicity of infection of 1 was used for all shPOLE experiments. The morning following infection cells were selected in puromycin or blasticidin for 3 days and then the media was changed and cells were allowed to recover for an additional day before being plated for experiments. Replating of cells for experiments occurred 5 days post infection. Lentiviral shRNA vectors were generated from the pLKO.1 backbone (RNAi consortium). Targeting sequences are provided in [Table S1](#). Doxycycline-inducible shPOLE\_1 generated by cloning shPOLE1\_1 shRNA sequence into Tet-pLKO-puro (Addgene 21915). Doxycycline-repressible NFS1 construct generated by cloning the NFS1 cDNA into pCW57.1. POLE1, POLE2, POLA1, and POLD1 genes were cloned into the pMXS-IRES-blast retroviral vector. ISC binding site mutations: POLA mutISC (C1348S, C1353S, C1371S, C1374S), POLD mutISC (C1348S, C1353S, C1371S, C1374S), POLE mutISC-POL (C651S, C654S, C663) and POLE mutISC-C (C2221S, C2224S, C2236S, C2238S). POLE cDNAs are N-terminal 3xFLAG tagged. POLE2 is N-terminal HA-tagged. Sequence information is available at: [https://www.addgene.org/Richard\\_Possemato/](https://www.addgene.org/Richard_Possemato/)

#### Proliferation Assays

Direct cell counts were performed using a Beckman Z2 Coulter Counter with a size selection setting of 8 to 30  $\mu$ m. For all drug withdrawal proliferation assays, 5000 cells were plated in sextuplets into 12-well plates before addition of drug the following day. At indicated withdrawal time points, three of six wells were counted, whereas for the rest of the wells drug was washed out and cells were cultured for indicated time points. Population doublings were calculated based on the ratio of cells at end of experiment to cell counts at time of withdrawal. For all other proliferation assays, 25,000 (MDA-MB-231, MDA-MB-468, HCC1954, MCF7, CAMA-1, EFM-19, SKBR3, T47D, MCF10A) or 50,000 (BT-20, BT-549, Hs578t, Zr-75-1) cells were plated in triplicate into 6-well plates for 5 days (MDA-MB-231, BT-549, Hs578t, HCC1954, MCF7, MCF10A), 7 days (MDA-MB-468, BT-20, EFM-19, SKBR3, T47D, ZR-75-1), or 9 days (CAMA-1). Media was changed on day 5 for all proliferation assays with a longer duration. Supplementation of pyruvate, uridine, and hypoxanthine for relevant experiments was started the day after infection. Viability assays were carried out by plating 1,000–2,000 cells in replicates of at least three in 96-well clear bottom plates (Greiner 655098) one day before adding the indicated drug. Viability was assessed by Cell Titer Glo (Promega) and normalized to an untreated control for each shRNA.

#### Cell Cycle Analysis

Cell cycle analysis was performed using and following the instructions of Click-iT Plus EdU Alexa Fluor 647 Flow Cytometry Assay Kit (C10634) from ThermoFisher. Briefly, cells were cultured for 1.5 hours in the presence of 10  $\mu$ M Edu before harvest, fixation, permeabilization and click-it reaction. After the following wash, cells were resuspended in 1X Click-iT saponin-based permeabilization and wash reagent containing 50  $\mu$ g/mL propidium iodide (PI) and 100  $\mu$ g/mL RNase A for at least 30 minutes. Data collection was performed on an Attune NxT Flow Cytometer with an excitation wavelength of 488 nm using the BL2 collection channel for PI and an excitation of 638 nm using the RL1 collection channel for Edu AF647 signal. Analysis of data was performed using FlowJo V.10 software.

#### Immunoblotting

Lysates collected on ice by washing cells in cold PBS followed by addition of lysis buffer (50 mM Tris pH 7.4, 150 mM NaCl, 1% NP-40, 0.1% sodium deoxycholate, 0.1% SDS, 2 mM EDTA) containing a protease inhibitor cocktail (Roche) and PhosSTOP. Lysates

were then incubated on ice for 10 min and sonicated for 10 s per sample in a cold room. Protein levels were quantified using a BCA protein assay kit (Pierce) and 8  $\mu$ g protein was loaded and electrophoresed onto Bolt 4%–12% Bis-Tris polyacrylamide gels (Thermo Fisher) or 3%–8% Tris-Acetate polyacrylamide gels (Thermo Fisher) for POLE detection. Gels were transferred onto a PVDF membrane (Millipore IPVH00010) in transfer buffer (2.2 g/L CAPS, 0.45 g/L NaOH, 10% ethanol) for 2 hours at 60V for Bis-Tris gels and 3 hours at 60V for Tris-Acetate gels.

### Immunopurification

500,000 HEK293 cells were plated and the following day transfected with 0.5  $\mu$ g of HA-POLE2 and 1  $\mu$ g of POLE or 0.5  $\mu$ g of POLD1 cDNA. After 16 hours, the media was changed and cells were collected 48 hours later, washed and lysed on ice in 1% NP-40, 150 mM NaCl, 1 mM EDTA, and 50 mM Tris pH = 7.5 containing 1X protease and phosphatase inhibitor for 15 minutes. Following the incubation, cells were spun at 13,000 rpm at 4°C for 10 minutes. 500  $\mu$ L of lysate was then transferred to 20  $\mu$ L of equilibrated slurry of Anti-FLAG magnetic beads and incubated in the cold room for 1.5 hours with rotation. Beads were pelleted, washed 3 times with lysis buffer, and then eluted with 60  $\mu$ L of 100  $\mu$ g/mL of 3X FLAG peptide. 15  $\mu$ L of elution diluted with SDS sample loading buffer was loaded per well.

### Aconitase Assay

Aconitase activity was measured using an Aconitase Assay Kit (Sigma, MAK051). 400,000–800,000 cells were plated in a 5-cm plate 5 days post infection. The next day cells were washed with PBS and harvested by trypsinization. To determine the aconitase activity of harvested cells, the manufacturer's protocol was followed without the addition of the activating solution.

### Correlations of Publically Available Data

Sensitivity scores were downloaded from <https://depmap.org/portal/download/all/> (Tsherniak et al., 2017). File Name: ExpandedGeneZSolsCleaned.CSV. A Pearson correlation was performed of ISCU sensitivity score to sensitivity scores of other genes across a panel of CCLE cell lines to produce a ranked list for Figure 2A. To obtain a ranked list of gene expression correlations to POLE suppression in breast cancer cell lines, CCLE expression data and sensitivity score data were filtered for breast cancer cell lines and a Pearson correlation was obtained between sensitivity score and gene expression. GSEA was performed using the ranked list with 1000 permutations and the curated gene sets (Subramanian et al., 2005).

### Non-Denaturing BrdU Assay

Cells were cultured in 10  $\mu$ M BrdU starting 2 days post infection and replated onto #1.5 glass coverslips in a 12-well plate 5 days post infection. BrdU immunostaining was performed on the following day as previously described (Mukherjee et al., 2015). Briefly, cells were washed with ice-cold PBS before nuclear extraction, fixation with 4% paraformaldehyde, permeabilization, and blocking. Coverslips were transferred to a humidifying chamber and primary incubation occurred overnight for 16 hours in 1:250 anti-BrdU (Abcam ab6326) diluted in 1% BSA. The following day, coverslips were washed, incubated with 1:500 Goat Anti-Rat IgG H&L (Alexa Fluor 594, ab150160) diluted in 1% BSA for 1 hr at room temperature, washed again and stained with DAPI. Coverslips were transferred onto glass slides containing a drop of mounting medium and sealed with transparent nail polish. Images were obtained on the Zeiss AxioImager.M1, and analysis was performed using ImageJ.

### DNA Fiber Assay

DNA fibers were prepared as described previously (Chen et al., 2015). Cells were pulsed with 50  $\mu$ M IdU and 50  $\mu$ M CldU for 20 minutes each for MDA-MB-231 and 30 minutes each for Hs578t and MCF7 cells. Cells were then harvested, washed in PBS, and resuspended at  $1 \times 10^6$  cells/mL in cold PBS for MDA-MB-231 and Hs578t cells and at  $0.5 \times 10^6$  cells/mL for MCF7 cells. 2  $\mu$ L of cells were transferred onto a glass slide and lysed with 10  $\mu$ L of lysis solution (0.5% SDS, 50 mM EDTA, and 200 mM Tris-HCl pH = 7.4) for 6 minutes. Slides were then tilted at a 15-degree angle to allow DNA spreading and air-dried in the dark. Afterward, slides were fixed for 2 min. in chilled, fresh 3:1 methanol:acetic acid, air-dried and stored overnight at 4°C. The following morning, the DNA was denatured with 2.5 N HCl for 30 min, washed with PBS, and blocked for 1 hr in 4% BSA dissolved in PBS containing 0.1% Triton X-100. Following blocking, the slides were stained for 1.5 hours with 1:150 anti-BrdU (Abcam ab6326) to detect CldU and 1:75 anti-BrdU (BD Bioscience 347580) to detect IdU. Next, slides were washed 3X in PBS and stained for 45 min. with secondary antibodies Anti-Mouse IgG Alexa Fluor 488 (CST, 4410) and Goat Anti-Rat IgG H&L Alexa Fluor 594 (Abcam, ab150160). Following secondary incubation, slides were washed 3X with PBS and coverslips were mounted on top of mounting medium and sealed with transparent nail polish. Images were obtained on the Zeiss AxioImager.M1, and analysis was performed using ImageJ. Tract length was calculated by measuring the length of CldU tracts adjacent to IdU tracts. At least, 90 tracts were measured for each individual sample in each independent experiment.

### qPCR

RNA was isolated by column purification (RNeasy Kit, QIAGEN) and cDNA synthesis was performed by reverse transcription of 1  $\mu$ g of total RNA by reverse transcriptase (Superscript IV, 18090010, Invitrogen) in a reaction containing 1  $\mu$ L RNase OUT (10777019, Invitrogen). qPCR was performed on cDNA using SYBR green quantification (Maxima qPCR master mix, K0222, Thermo Fisher). All genes part of Table S1 were quantified relative to ACTB, and qPCR primer information for these genes can be found in the table.

*IL1A*, *IL1B*, *IL6*, *CSF3*, *CDC25A* were quantified relative to *RPL13A*. The following primers not listed in Table S1 were used: *ACTB* forward: AAGGGACTTCC TGTAACAATGCA, *ACTB* reverse: CTGGAACGGTGAAGGTGACA, *RPL13A* forward: CATA GGAAGCTGGGAGCAAG, *RPL13A* reverse: GCCCTCCAATCAGTCTTCTG; *IL1A* Forward: AGACCAACCAGTGCTGCTGA, *IL1A* Reverse: GGATGGGCAACTGATGTGAA, *IL1B* Forward: CTGAGCTCGCCAGTGAAATG, *IL1B* Reverse: GGTGGTCGGAGATTCGTA GC, *IL6* Forward: AAGCCAGAGCTGTGCAGATG, *IL6* Reverse: GCTGCGCAGAATGAGATGAG, *CSF3* Forward: TCTGGCAGCAGAT GGAAGAA, *CSF3* Reverse: ACACCTCCAGGAAGCTCTGC, *CDC25A* Forward: CACCAACCTGACCGTCACTA, *CDC25A* Reverse: GTTCTTCACCTCCAGTGGTTG, *POLE2* Forward: CTTTGGATTCCACCCACTG, *POLE2* Reverse: TTTTGCAGAAGTCTTCACA GATG.

### Senescence Associated $\beta$ -Galactosidase Assay

Cells were washed with PBS and then fixed using 0.2% glutaraldehyde for 5 min. at room temperature. Next, cells were washed twice with PBS and then stained with X-gal solution (1mg/mL X-gal, 150mM NaCl, 2mM MgCl<sub>2</sub>, 5mM K<sub>3</sub>Fe(CN)<sub>6</sub>, 5mM K<sub>4</sub>Fe(CN)<sub>6</sub>, 40mM NaP<sub>i</sub> pH = 6.0) overnight at 37°C in a non- CO<sub>2</sub> incubator for 16 hours. After staining, cells were washed with PBS and the plate was stored at 4°C.

### RNaseq

RNA was isolated using the RNeasy Plus Mini Kit. Analysis was done with normalized read counts. GSEA was performed with 1000 permutations in the curated gene sets.

### Phosphoproteomics Data Analysis

Phosphoproteomics data used in this publication were generated by the Clinical Proteomic Tumor Analysis Consortium (NCI/NIH); the CPTAC\_BCProspective\_BI\_Phosphoproteome\_CDAP\_Protein\_Report.r1 was downloaded from <https://cptac-data-portal.georgetown.edu/study-summary/S039>. A list of putative CDK1/CDK2 targets was downloaded from PhosphoSitePlus (<https://www.phosphosite.org/homeAction.action>) (Hornbeck et al., 2012). Phosphoproteomics data was preprocessed by removing samples for which fewer than 10,000 phosphopeptides were measured, then removing phosphopeptides for which fewer than 25% of remaining samples were measured. Samples were then quantile normalized (Bolstad et al., 2003). To measure enrichment in basal samples over luminal samples, all phosphopeptide values were transformed with  $2^{\text{value}}$  to recover relative abundance ratios. Ratios were then averaged separately for basal and luminal samples (LumA and LumB). We then calculated the log<sub>2</sub> of the ratio of mean basal values over mean luminal values for all sites. CDK1/2 targets were compared against non-targets using the rank sum test from Scipy (Virtanen et al., 2020). To find phospho sites enriched in basal versus luminal samples, we used the rank sum test from Scipy (Virtanen et al., 2020) on proteome-wide phosphopeptide abundances, comparing basal versus LumA and LumB abundances. Rank sum p values were corrected using the bonferroni correction (Bonferroni, 1936) from statsmodels (Seabold and Perktold, 2010). Pandas (McKinney, 2010) and numpy (Oliphant, 2006; van der Walt et al., 2011) were used for data handling; matplotlib (Hunter, 2007) and seaborn (Waskom et al., 2017) were used for visualization.

### QUANTIFICATION AND STATISTICAL ANALYSIS

Experiments were repeated at least three times with the following exceptions: RNaseq was performed on two biological replicates per condition, ShRNA suppression screen of 14 ISC DNA Metabolism in 4 breast cancer cell lines performed once (Figure S2C) although multiple targets were further validated, Time course for second single cell clone part of Figures S1E and S2F, qPCR to validate POLE2 knockdown in Figure S2I and CDC25A knockdown in Figure S4J. P values reported in the figures are the result of Student's t tests and distributions assumed to follow a Student's t distribution. These assumptions are not contradicted by the data. No samples or animals were excluded from analysis and sample size estimates were not used. The number of independent biological replicates (n) are indicated in the figure legend and represent replicate measurements from distinct samples. For immunoblots and autoradiography, the reported images are representative of at least three independent experiments. Studies were not conducted blind.